POLITECNICO DI MILANO
School of Industrial and Information Engineering
Master of Science Course in Aeronautical Engineering

Numerical simulation of laser-gas interaction in a microchannel

Supervisor: Prof. Aldo Frezzotti

Master Thesis of:
Filippo Gorletta
905185

Academic Year 2020-2021

Contents

List of Figures

List of Tables

Nomenclature

$\bar{\tau}$	Stress tensor
ℓ	Characteristic length
λ	Mean free path
$\mathbf{\Psi}$	Vector of conserved variables
$\mathbf{U}$	Velocity
μ	Dynamic viscosity
ϕ	mass flow rate
Φ_f	Volumetric flux
Φ_q	Thermal flux
ρ	Density
A_s	sutherland constant
Ar	Argon
c	Speed of sound
c_p	specific heat
e	Energy
f	Frequency
k	Thermal conductivity
Kn	Knudsen number
M	Mach number

P	Pressure
r	Ratio of successive gradients
Re	Reynolds number
T	Temperature
T_s	sutherland constant
$t_{1/2}$	half-life

Sommario

In questo lavoro viene analizzato il comportamento di un gas nobile (Argon) all'interno di un micro canale quando viene investito da un raggio laser della durata di $10^{-15}s$ per la produzione di XUV (extreme ultraviolet radiation). La geometria semplificata non include i canali di alimentazione del dispositivo reale, ma solo il micro canale cilindrico principale che viene utilizzato come guida d'onda cava. L'attenzione viene focalizzata sui fenomeni legati alla gasdinamica che avvengono all'interno del canale, in modo da comprendere, tramite la simulazione numerica di OpenFOAM, la propagazione delle onde d'urto, i tempi caratteristici di svuotamento e le ulteriori possibili semplificazioni alla geometria. In una prima fase viene analizzato il problema e il set up dell'esperimento, successivamente ci si concentra sullo svuotamento del canale e sui fenomeni che lo influenzano. Si prevede che, cambiando la geometria o il set up dell'esperimento, si possano accorciare i tempi di svuotamento andando incontro alla richiesta di avere uno svuotamento completo in scala di tempo di $10^{-5}s$. Ulteriori test verranno eseguiti per valutare i carichi sulle pareti del canale e i relativi flussi termici.

Abstract

In this work Argon behaviour inside a micro channel is analysed when a laser pulse of $10^{-15}s$ hits the gas for XUV (extreme ultraviolet radiation) production. The simplified geometry does not include the network of gas delivery micro channels but only the main cylindrical micro channel that acts as a hollow waveguide. Attention is payed on gasdynamic phenomenas that occur inside the micro channel in order to understand, through OpenFOAM numeric simulation, shock waves propagation, emptying process characteristic time and possible further simplifications to the geometry. At first, the problem and the experiment set up is analysed, then the work will move on predict the channel emptying time and the phenomena that can influence this process. It is expected that, changing the geometry or laser set up, emptying time can be shortened matching the request of a complete emptying process within the time scale of $10^{-5}s$. More tests are done to evaluate pressure on the channel wall and relative heat fluxes.

Chapter 1

Introduction

1.1 Motivations

The aim of this thesis is to understand the behaviour of a chosen gas in a cylindrical micro channel ($r < 1mm$) when heated by a laser beam with a Gaussian power profile ($400 - 500\mu J$) . It has been observed that an intense femtosecond laser pulse focused in a gas medium drives the emission of a burst of coherent radiation, collinear to the driving beam, its spectral content range from the vacuum ultraviolet to the soft x-rays [5].
This process is called high-order harmonic generation (HHG) since the spectrum of emitted radiation appears as a combination of odd harmonics of the fundamental laser field. The idea is to use HHG as a source for extreme ultraviolet (XUV) spectroscopy and provide a relevant technology for studying ultrafast dynamics in atoms, molecules and condensed matter with temporal resolution of on the attosecond time-scale [2]. The understanding of whole system is not the main subject of this work, the important part is to fully describe the gas dynamic inside the channel.
The micro channel is filled with Argon at prescribed pressure and density through multiple supersonic inlet, this allow to tune the density properly in order to obtain a gradual decrease towards the outlets, a cylindrical section of this gas is then heated by a laser beam to increase drastically temperature, thanks to short duration of the pulse the power peaks becomes intense even for low pulse energies. A strong discontinuity occurs inside the channel and a cylindrical shock wave propagates in radial direction, meanwhile the gas starts expansion in vacuum through two outlet placed at the extremity of the micro channel. After that a new injection of Argon and a new laser impulse are provided. The numerical analysis is necessary in order to appreciate the characteristic time of cylindrical shock wave propagation, to estimate the

emptying time and exhaust volumes characteristics.
About micro channel fabrication, that is not a topic of this work, it is reported that to achieve this kind of miniaturization is required a femtosecond laser micromachining that is a powerful fabrication technique frequently used in the lab-on-chip devices. The chosen one is the FLICE technique, it consist in two step, the first one involve the irradiation of the sample with focussed femtosecond laser pulses, then the following part is etching of the laser modified zone by a hydrofluoric acid (HF) solution in water. This approach allows better accuracy, flexibility and 3D capabilities for guiding laser beams through micro channel [3].

1.2 Main targets

To perform the study described some simplifications on the geometry are needed, the original problem is much more complex than the one presented. First of all the real micro channel used in the experiments has a 3D geometry that is not reported here, a simple cylinder is used; the gas delivery channels and the hollow waveguide are not represented and the attention is focused on what happen in the channel after the laser is switched off. The attention must be focused on different elements, first of all the critical aspect of the simulation, due to laboratory set up, is the frequency at which laser can operate, it has a maximum and it is $f = 100kHz$.
This information influences significantly the experiment since the gas had to fully expand and leave the channel. Since it is difficult to forecast gas temperature starting from laser pulse power, it is better to treat temperature as a parameter and perform the study on different temperature sets.
The intention is to dimension the channel to figure out if the second laser impulse hits *fresh new* gas coming from delivery channels or still expanding one, in this case new trial are carried out and some advice on possible solution are given.
Another important aspect is to figure out if radial and axial motions happen in two different time scale. If the characteristics time of the phenomenas are distinct a further consideration should be made: the motion should be decoupled bringing to an easier problem. As a least point it should be done an analysis on the pressure maximum reach on the chip and on the heat flux during the whole simulations as a starting point for future work.

1.3 Thesis structure

In the first part of the thesis the main goal is to understand the problem, from every point of view starting from the hypothesis that are made to simplify the analysis.
In the first chapter attention is payed to fully picture the system, a description of the set up is given along with a complete analysis on the gas characteristics, so what kind of flow in expected. Governing equations and mathematical models of the flow are declared with a brief description of high temperature gas effects and hypersonic flows.
A description of the software used for this work and all the embedded utilities is made. Main focus is given to problem set up and to mesh generation, but also to describe in detail the software. The final part deals with results of the numerical simulations, comment on the possible solution and future development.

Chapter 2

Problem Definition

The second chapter of this work describes the modelling of the problem with accuracy but also without overcomplicate the system. This case involves an high-ethalpy gas (over $1000K$) in a micro channel, it is important to introduce some hypothesis to fully acknowledge the physics of the problem and to work with the correct tools in the numeric simulation.
In this simulations channel is filled with Argon (Ar), a noble gas of third period that can be found in air and compose 0.95% of the Earth's atmosphere. It is chosen in this experiment because it is extremly stable and its thermophysical properties slightly change at very high temperature. In figure 2.1 is reported the electronic configuration.

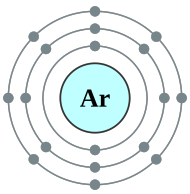

Figure 2.1: Argon atomic structure

Argon	
Simbol	Ar
Phase at STP	gas
Atomic Number	18
Atomic weight	39.95

Table 2.1: Argon properties

2.1 Hypothesis

The problem must be understood from the point of view of flow regime, in this experiment Argon is provided through supersonic inlet to allow a density tuning in the channel, Knudsen number is the main parameter to understand if the flow can be considered a continuous media. The separation of length scale is quantified by the Knudsen number

$$Kn \equiv \lambda/\ell \tag{2.1}$$

in general we have the following situations:

- $Kn << 1$ viscous regime, the continuum approach is appropriate. Flow well described by Navier-Stokes equations.
- $Kn >> 1$ free molecular path regime, motion of the single molecule is independent from the other, molecular collision are neglected.
- $0.01 < Kn < 1$ transitional regime, the correct approach is a stochastic one such as Direct Simulation Monte Carlo that solve Boltzmann equation, molecular collision can't be neglected and the continuum approach is not correct.

In equation 2.1 ℓ represents the characteristic length of the problem, here the diameter of the micro channel, λ is the mean free path, so the mean distance that a molecule can travel without clashing into another molecule [9]. For this problem the Knudsen number is:

$$Kn = \frac{3.28 \times 10^{-7} m}{2 \times 10^{-4} m} = 1.64 \times 10^{-3} \tag{2.2}$$

The regime is viscous and the continuum approach is the chosen one.

Due to high pressure and temperature gradients in radial direction, particular attention should be payed to flow characteristics and, in particular, to understand if it is possible to consider the flow compressible or incompressible. The Mach number is defined as the ratio between the flow velocity and the local speed of sound

$$M = \frac{U}{c} \tag{2.3}$$

it is a good indicator of the simplifications that could be adopted, if $M < 0.3$ flow can be considered incompressible, but it is not the case presented here since in the first moments of the simulation flow velocity increases

rapidly reaching $M = 1$, so the shock propagates with supersonic velocity and the flow is treated as compressible. The cylindrical shock wave propagates in radial direction, after bouncing back and forth it decreases its intensity, this part will be analysed in detail in subsequent sections, the problem is of course unsteady.

Viscosity is another important feature of a gas and the parameter that define its importance is the Reynolds number. It represent the ratio between inertia forces and viscous forces

$$Re = \frac{\rho U L}{\mu} \tag{2.4}$$

In this case the diameter of the channel is the characteristic length, velocity and density are taken at the outlets. In a preliminary study it can be seen that even with a sonic flow the regime is laminar since $Re = 210$ is very low, approximately.

To resume flow characteristic:

- Continuum approach is correct for $Kn << 1$
- Compressible flow
- Laminar regime
- Unsteady simulation

2.2 Governing Equations

The governing equations for a viscous flow are presented, the so called *Navier-Stokes equation.*
Continuity Equation:

$$\frac{\partial \rho}{\partial t} + \nabla \cdot (\rho \vec{u}) = 0 \tag{2.5}$$

Momentum Equation:

$$\frac{\partial \rho \vec{u}}{\partial t} + \nabla \cdot \left(\rho \vec{u} \otimes \vec{u} + P\bar{I} - \bar{\tau} \right) = 0 \tag{2.6}$$

Energy Equation:

$$\frac{\partial \rho e}{\partial t} + \nabla \cdot \left(\rho e \vec{u} + P\bar{I} \cdot \vec{u} - \bar{\tau} \cdot \vec{u} + \vec{q} \right) = 0 \tag{2.7}$$

where:

$$P = \rho RT \qquad \tau_{ij} = \mu\left(\frac{\partial u_i}{\partial x_j} + \frac{\partial u_j}{\partial x_i}\right) - \frac{2}{3}\mu\delta_{ij}\nabla \cdot \vec{u}$$

$$e = c_v T \qquad \vec{q} = -k\nabla T$$

The need for a compressible solver for our simulations is straightforward, Mach number in fact is approximately one at the end of the channel (the flow is sonic), and greater than one in the low pressure chamber. High pressure and temperature gradients are present and phenomena such as expansion fans, shock waves and contact discontinuity must be well represented.

2.3 Laser-Gas interaction

In this experiment the femtosecond laser hits a portion of Argon inside the channel, the power of the laser is $5mJ$ but for this so short period of time generates a large amount of energy. This physical effect is called high harmonic generation and occurs when an atomic gas is placed in a laser field and emits photons at frequencies of integer multiples of the driving field frequency, HHG is used as a promising source for extreme ultraviolet (XUV) and the main uses could be photoelectron spectroscopy, solar imaging and lithography. [2]
Model with accuracy laser-gas interaction is not the main concern of this work, ionization phenomena occurs but are not taken into account since extinguish rapidly and do not affect flow behaviour [8]. When the simulation start the laser beam with a radius of $2.25 \times 10^{-5}m$ has already hit the portion of Argon and change drastically its temperature and pressure, but density and velocity magnitude remain unchanged; this means that laser-gas interaction is modelled as a initial discontinuity in pressure and temperature. From this strong discontinuity radial cylindrical shockwave propagates but drops in a short time compared to the channel emptying process, this behaviour will be discussed in chapter 4

Chapter 3

Methodology

The simulation are run on a Xeon Phi processor available at Aerospace Department of Politecnico di Milano, there are two of them called *Castore* and *Polluce*. Each computer features a developer Edition of Intel Xeon Phi processor with 64 cores with 4 threads clocked at 1.30 GHz and 16 GB of MCDRAM, the simulation are performed on *Castore* using all the 64 physical cores, unfortunately is not possible to exploit hyper-threading using $64 \times 4 = 256$ cores this is due memory access issue and bandwidth consideration that go beyond the main topic of this work.

3.1 OpenFoam ®

Computational fluid dynamics is focused on the prediction of fluid motion and forces by computation using numerical analysis, including heat, thermodynamics, chemistry and solids [4]. The main target is to solve partial differential equations (PDEs), in this case the conservation laws introduced in section 2.2 that govern the fluid motion. The PDEs are represented as a set of algebraic equations at discrete point in the solution domain, the numerical method chosen is the popular *finite volume method* in which the solution domain is subdivided into a mesh of small volumes, also called cells. Fluid dynamic quantities are centered on the control volume centroids (P and N in figure 3.1), a variety of available interpolation and discretization solution scheme can be selected.

The software chosen is OpenFOAM (Open Field Operation And Manipulation), it is a C++ toolbox that, thanks to a collection of more than 100 C++ libraries, can deal with different problems in fluid dynamics; there are three principle OpenFOAM versions and for this work the OpenFOAM-

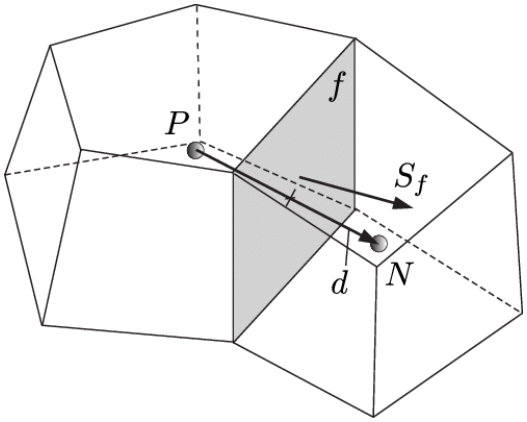

Figure 3.1: Finite volume method

fundation fork is the selected one.
OpenFOAM contains approximately 250 pre-built applications that can be divided in two categories: *solver* that are designed to solve a specific problem in fluid dynamics and *utilities* that perform specific tasks, such as data manipulations.
The software is shipped with pre- and post-processing environments, they are indeed OpenFOAM utilities that ensure consistent data handling across all platform. The overall structure is described in figure 3.2a.

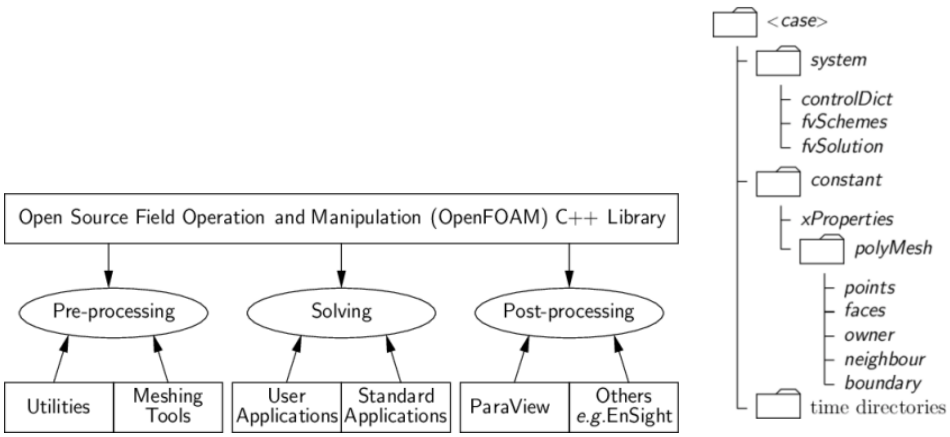

(a) *Overview* (b) *Case structure*

The first thing to analyse is the case set up, the input data includes time information (start time, end time and time step), setting numerical schemes, matrix solver and algorithm controls; all these features are crucial since affect

computational time and solution stability. To better understand a directory structure for an OpenFOAM case we can observe figure 3.2b, a `constant` directory contains a full description of of the case mesh in a subdirectory called `polymesh` and files specifying physical and transport properties. The `system` directory contains the following text files:

- *controlDict* where run control parameters are set such as start/end time, time step and data format.
- *fvSchemes* where discretization scheme is selected.
- *fvSolution* where the equation solvers, tolerances and other algorithm controls are set.
- *blockMeshDict* where the mesh is fully described and, thanks to the utility `blockMesh`, created.
- *setFieldsDict* where it can be defined a region with different initial condition for scalar and vector fields, it is necessary to launch the utility `setFields`.
- *decomposeParDict* where the solution domain is subdivided in n parts so that parallel computation can be handled. Each part of the domain is adressed to a specific processor and with the utility `decomposePar`.

As mentioned above, OpenFOAM uses dictionaries as common means of specifying data, dictionary is an entity that contains data entries that are called by the I/O by means of keywords. The general structure is;

```
<dictionaryName>
{
<keyword>  <dataEntry>;
}
```

Most applications contain list, e.g a list of vertex cordinates for mesh description. All the entries are contained between round braces:

```
<ListName>
(
   ...entries...
);
```

3.2 Solver and utility description

The problem analysed here involve shock waves, for this reason a shock-capturing method is needed, without going into deep theory, it is sufficient to say that in these methods the governing equations are cast in conservation form and any shock waves or discontinuities are computed as part of the solution. The selected solver for our simulations is `rhoCentralFoam`, a compressible and density based solver. The presence of sock waves in high-speed compressible flow requires a numerical schemes that can capture these features avoiding spurious oscillations. This solver does not involve Riemann solvers of characteristic decomposition and can avoid Jacobian evaluation, it is a central scheme that provide a non-oscillatory solution thanks to a second-order generalization of the Lax-Friedrichs scheme.
Application of Finite Volume method starts by expressing the differential equations with an integral over a cell volume V, divergence term are converted to surface integrals using the divergence theorem and evaluated as fluxes at the surfaces evaluated by interpolation of cell centre values to the faces, in order to complete this discretization it is used a central-upwind scheme of Kurganov, Noelle and Petrova.
The solution procedure in rhoCentralFoam begin with a directed interpolation of primitive fluxes onto faces and, eventually, making fluxes relative to mesh-motion, then continuity and momentum equation are solved updating density and velocity. After that rhoCentralFoam start solving energy equation with eventual coupled terms (combustion and chemistry), pressure is updated along with turbulence model and thermophysical properties (figure 3.2).

Finite volume description and shock capturing scheme

3.2.1 Constant directory

Inside this directory it is possible to find two important text files that solver need to handle the problem, `momentumTransport` and `thermophysicalProperties`. The first one is a dictionary that includes a turbulence modelling, for all the simulation it is set:

```
simulationType      laminar;
```

This is due to the low Re inside the channel that result in a laminar flow. The second dictionary is about thermophysical models that are concerned with energy, heat and physical properties; a thermophysical model is constructed in OpenFOAM as a pressure-temperature system from which

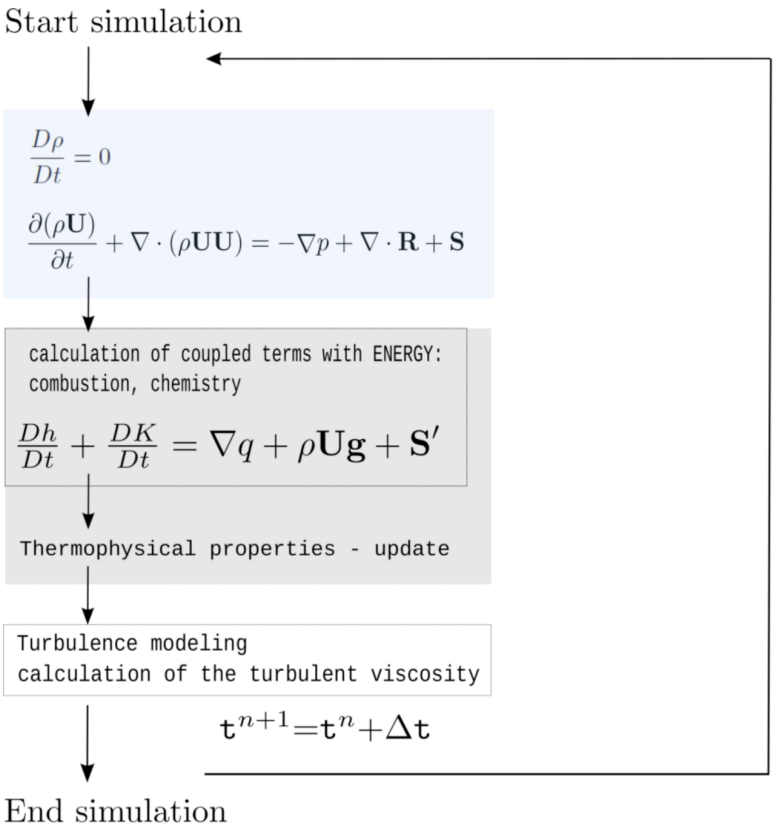

Figure 3.2: rhoCentralFoam solution procedure

other properties are computed. The compulsory dictionary entry called `thermoType` specify the package of thermophysical modelling used for the simulations. The coding approach is simple, every package begin with the equation of state and then more layers are added with desired properties in order to improve the model.

```
thermoType
{
    type            hePsiThermo;
    mixture         pureMixture;
    transport       sutherland;
    thermo          hConst;
    equationOfState perfectGas;
    specie          specie;
    energy          sensibleInternalEnergy;
}
```

The thermo type `hePsiThermo` is used for fixed composition (argon is the only gas present in the channel) and it is based on compressibility $\psi = (RT)^{-1}$ where R is the gas constant and T the temperature. Keyword `pureMixture` indicates a models without chemical reactions. The evaluation of dynamic viscosity μ, thermal conductivity κ and thermal diffusivity α can be done through *Sutherland model*

$$\mu = \frac{A_s\sqrt{T}}{1 + T_s/T} \tag{3.1}$$

the coefficient values are defined in the mixture dictionary where also gas properties are inserted

```
mixture
{
    specie
    {
        molWeight       39.948;
    }
    thermodynamics
    {
        Cp              520.3;
        Hf              0;
    }
    transport
    {
      As            2.209e-06;
      Ts            166.4;
    }
}
```

Constant terms as A_s and T_s are taken from [1] thanks to MATLAB tool curve fitting, equation 3.1 is taken as reference, coordinates are known and the tool extracts constant term with enough accuracy. Thermodynamic model assumes a constant c_p as it can be seen from table in [1], in this particular case it will be unnecessary complication adopt JANAF model in which c_p is taken as function of T from a set of coefficient, but it is correct to state:

$$c_p = \frac{5}{2}R \tag{3.2}$$

3.2.2 fvSolution and fvSchemes

Other important dictionaries are `fvSchemes` and `fvSolution`, the first one contains the numerical scheme for terms such as derivatives in equations and the second one contains equation solvers, algorithms and tolerances of the simulations.
In `fvSchemes` user can custom the discretization and interpolation scheme, the set of terms for which numerical scheme must be specified are:

- `ddtScheme` first and second time derivative
- `gradScheme` gradient ∇
- `divScheme` divergence $\nabla\cdot$
- `laplacianScheme` laplacian ∇^2
- `interpolationSchemes` cell to face interpolation scheme
- `snGradSchemes` component of gradient normal to a cell face
- `wallDist` distance to wall calculation

The keyword selected for all cases are

```
fluxScheme      Kurganov;

ddtSchemes
{
    default         Euler;
}
gradSchemes
{
    default         Gauss linear;
}
divSchemes
{
    default         none;
    div(tauMC)      Gauss linear;
}
laplacianSchemes
{
    default         Gauss linear corrected;
}
```

```
interpolationSchemes
{
    default         linear;
    reconstruct(rho) vanAlbada;
    reconstruct(U)  vanAlbadaV;
    reconstruct(T)  vanAlbada;
}
snGradSchemes
{
    default         corrected;
}
```

Convective terms are critical in central schemes as rhoCentralFoam, in fact for compressible flows fluid properties are not only transported by the flow, but also by the propagation of waves. This requires the flux interpolation to be stabilized based on transport that can occur in any direction. The selected method is the Kurganov flux for multi-dimensional system using the dimension-by-dimension recontstruction (for detail see [6]). The treatment of convective term is now presented:

$$\int_V \nabla \cdot (\mathbf{u}\boldsymbol{\Psi})\, dV = \int_S d\mathbf{S} \cdot (\mathbf{u}\boldsymbol{\Psi}) \approx \sum_f \mathbf{S}_f \mathbf{u}_f \boldsymbol{\Psi}_f = \sum_f \Phi_f \boldsymbol{\Psi}_f \tag{3.3}$$

the pedix f denotes a summation over cell faces and $\Phi_f = \mathbf{S}_f \mathbf{u}_f$ is the volumetric flux. As it is said before, linear interpolation is not correct, it is mandatory to interpolate splitting into two main direction, flow that is going outward f_- and flow that is going inward f_+ of the face owner cell. So it becomes:

$$\sum_f \Phi_f \boldsymbol{\Psi}_f = \sum_f \left[\alpha \Phi_{f_+} \boldsymbol{\Psi}_{f_+} + (1-\alpha) \Phi_{f_-} \boldsymbol{\Psi}_{f_-} + \underbrace{w_f \left(\boldsymbol{\Psi}_{f_-} - \boldsymbol{\Psi}_{f_+} \right)}_{\text{diffusion term}} \right] \tag{3.4}$$

The third term is a diffusion term using a volumetric flux w_f based on the maximum speed of propagation of any discontinuity that may exist at a face between values interpolated in the f_+ and f_- directions. Coefficient α can be wighted equally or can be based on one-side local speeds of propagation:

$$\alpha = \begin{cases} 0.5 & \text{for Kurganov and Tadmor} \\ \dfrac{\psi_{f_+}}{\psi_{f_+} + \psi_{f_-}} & \text{for Kurganov Noelle and Petrova} \end{cases} \tag{3.5}$$

Where volumetric fluxes associated with the local speeds of propagation are:

$$\psi_{f_\pm} = \max\left(c_{f_+}\left|\mathbf{S}_f\right| \pm \psi_{f_+},\, c_{f_-}\left|\mathbf{S}_f\right| \pm \psi_{f_-},\, 0\right) \tag{3.6}$$

$$c_{f_\pm} = \sqrt{\gamma R T_{tr_{f_\pm}}} \tag{3.7}$$

The last equation represents the speeds of sound at the gas face, outward and inward of the owner cell.

As interpolation scheme is chosen `vanAlbada`, flux at cell faces can be represented by low and high resolution scheme. The main idea is to think high order flux as consisting of the low order flux plus a correction, this is done because low order flux contains too much diffusion and works well near discontinuities, but not so well in smooth region. In order to switch between low and high order scheme the interpolation procedure uses a flux limiter function $\beta(r)$ where r represents the ratio of successive gradients for the interpolated variable, this is the best way to understand if a discontinuity is present.

$$\beta(r) = \frac{r + r^2}{1 + r^2} \quad \text{for van Albada} \tag{3.8}$$

The numerical scheme of Kurganov Noelle and Petrova has two important advantages, first it does not rely on the specific eigenstructure of the problem, second the interpolation of values depends solely from owner cell and a neighbouring cell. However the main disavantage is its dissipative nature, so it requires a superior quality mesh, in particular where the shock waves arise.
For gradient, divergence and laplacian schemes it is used the standard finite volume discretization of Gaussian integration, corrected in case of non-orthogonal meshes, this is not the case since it is used a structured mesh.
In `fvSolution` dictionary the equation solvers, tolerances and algorithms are controlled, here is reported the file structure:

```
solvers
{ "(rho|rhoU|rhoE)"
    { solver          diagonal;}
    U
    {   solver          smoothSolver;
        smoother        GaussSeidel;
        nSweeps         2;
```

```
        tolerance       1e-09;
        relTol          0.01;}
    h
    {   $U;
        tolerance       1e-10;
        relTol          0;}
    e
    {   $U;
        tolerance       1e-10;
        relTol          0;}
}
```

rhoCentralFoam is an explicit solver, to solve matrix equation it is necessary a diagonal linear solver that gives the exact solution of the linear system for ρ. The Gauss-Seidel method is an iterative method use to solve system of linear equations, it is used for U, h and e.

3.2.3 controlDict

This dictionary is a database that controls I/O setting input parameters essential for the simulations, the `controlDict` dictionary was modified during different tests in order to obtain different timing of write output to file or to include different functions, but the general structure is the following:

```
application     rhoCentralFoam;
startFrom       startTime;
startTime 0;
stopAt          endTime;
endTime         1e-4;
deltaT          1e-10;
writeControl    adjustableRunTime;
writeInterval   1e-5;
cycleWrite      0;
writeFormat     ascii;
writePrecision  6;
writeCompression off;
timeFormat      general;
timePrecision   6;
runTimeModifiable true;
adjustTimeStep  yes;
maxCo           0.7;
maxDeltaT       1e-8;
```

the most modified parameter across simulations are `endTime` and `writeInterval` in order to study different phenomena of the flow field, for instance radial shockwave has a characteristic time very low compared to the emptying channel.

The flow is unsteady and particular attention must be payed to time step and to final time, rhoCentralFoam is an explicit solver that need a little time step to fully capture flow behaviour, the Courant number is consider to help select an adaptive time step:

$$Co = \frac{|\mathbf{U}|\,\Delta t}{\Delta x} \tag{3.9}$$

this quantity must be less than 1, this is a necessary condition (not sufficient) for stability and convergence, if a perturbation propagates with velocity $\mathbf{U}$, the temporal resolution Δt must be smaller than $\frac{\Delta x}{|\mathbf{U}|}$ that represent the time of propagation of the perturbation [7]. In other words temporal resolution must be smaller than characteristic time of the phenomena. This means $Co < 1$, to achieve this target it is chosen $\Delta t = 10^{-10}s$. It is worth notice that the flag `adjustTimeStep` is active, this means the solver evaluate the mean and max Courant number adjusting the time step keeping a value of $Co \leq 0.7$

3.2.4 setFieldsDict

It is a practical dictionary to specify non-uniform initial condition, it is adopted to model the low-pressure expansion chamber and the laser-gas interaction, in fact at starting time laser has already hit a portion of gas increasing pressure and temperature locally. `setFieldsDict` entries are here reported:

```
defaultFieldValues
(
    volScalarFieldValue T 300
    volScalarFieldValue p 41572
);
regions
(
    cylinderToCell
    {
        p1        (0 0 0);
        p2        (0 0 0.003);
        radius    2.25e-5;
```

```
        fieldValues
        (
            volScalarFieldValue T 12000
            volScalarFieldValue p 1662800
        );
    }
    cylinderToCell
    {
        p1      (0 0 0.003);
        p2      (0 0 0.04);
        radius  1.3e-3;
        fieldValues
        (
            volScalarFieldValue p 100
            volScalarFieldValue T 300
        );
    }
);
```

The utility `setFields` need to be launched after mesh generation and, in the declared regions, overrides the default values with `fieldValues`.The topological constraint is a cylinder that define a set of cells where temperature and pressure are modified.

3.2.5 decomposePar

This dictionary is used to decompose mesh and fields of a case for parallel execution, OpenFOAM case run in parallel using the openMPI implementation of MPI. The main idea is to assign at each processor separate pieces of the domain and compute an economic solution. The geometry and field are broken according to a set of parameter specified in `decomposeParDict`:

```
numberOfSubdomains 64;
method          scotch;
```

As said at the beginning of the chapter the physical cores are all used, the decomposition uses the scotch method, this requires no geometric input from the user and attempts to minimise the number of processor boundaries, so the boundaries between different parts of the mesh. After the mesh is built and setFields run, before starting the simulation the user need to run `decomposePar` creating different folders named *processor0, processor1,*

... with field data, when the simulation ends the user needs to run the command `reconstructPar` to build up the final solution.

The aim of this sub-sections is simply introduce the software and its structure, not every feature is discussed here or in the next paragraphs, for further information consult the User Guide [4].

3.3 Mesh Generation

The utility `blockMesh` deserves a dedicated section, in fact in computational fluid dynamic one of the first thing to focus on is the mesh generation. In order to reduce computational effort it is possible to exploit the axi-symmetry of the problem, the simulation domain is a cylindrical pipe with diameter $200\mu m$ and length $6mm$. Through the utility `blockMesh` it is possible to create parametric meshes with grading and curved edges. This utility reads the `blockMeshDict` dictionary, generates the mesh and writes in `constant/polyMesh` directory mesh data to points, faces and boundary files.
The idea is to decompose the solution domain in a set of hexahedral blocks, these blocks are defined by 8 vertices written in a list:

```
blocks
(
    hex (0 1 2 3 4 5 6 7)   // vertex numbers
    (10 10 10)              // numbers of cells xyz direction
    simpleGrading   (1 1 1) // cell expansion ratios
);
```

In this study a pair of vertices need to collapse onto each other to create the geometry of a small angle wedge (see figure 3.3)

```
hex (0 1 2 0 3 4 5 3)
```

The problem involve a simple geometry, a small cylindrical channel connected to a sufficiently large low-pressure chamber where gas will expand (figure 3.5). As mentioned before, computational cost need to be carefully considered, exploiting axi-symmetry and symmetry with respect to z-plane (plane placed at the half of the channel and with normal going in z-direction) it is convenient to run simulation in one half of the channel. There is no need for an unstructured grid, it is preferred a structured one (figure 3.4) that can be refined in the radial direction to fully capture cylindrical shock waves and

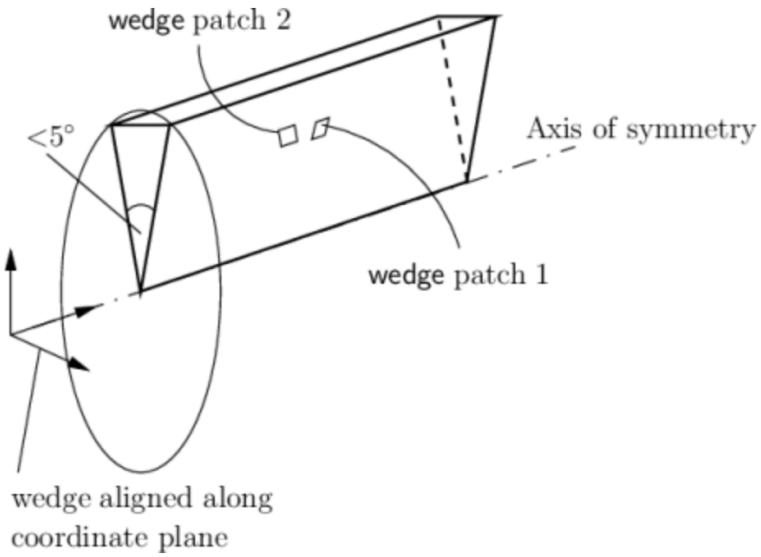

Figure 3.3: Axi-symmetric geometry using wedge patch type

temperature gradient. Along the axis it is mandatory to find the trade off between computational cost and solution refinement, for these reasons some grid convergence run are carried out.

3.3.1 Radial grid convergence

Two types of phenomena occurs in this problem, the fastest one is the cylindrical shock waves that develop for the initial jump in pressure and temperature, then after a few μs the pipe starts emptying through two outlets. It is important to fully describe both the events and to capture the correct shock development, for this reason some grid convergence run are done.
In this section we will focus on radial direction, simulation are run until $1\mu s$ and results at latest time are compared to find right refinement to capture this *fast* phenomena; particular attention is payed in what happen inside the channel, for this reason the mesh selcted is slightly different from the previous presented: there is no need for a chamber where gas expands, so the ends of the cylinder are no more outlets but walls where a *slip* condition is set. The mesh is going to be refined in radial direction in order to have *long slices* of the channel and to capture flow behaviour 3.7

Six simulations are done until invariance of the result is reached.

For completeness more simulation are run, it is reached a number of cell

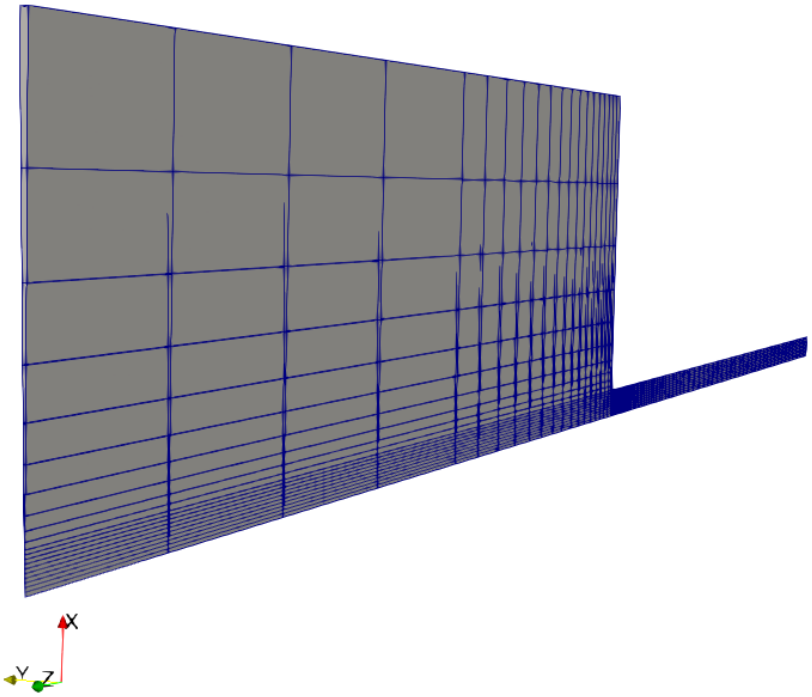

Figure 3.4: Mesh used for the simulations

Simulation	n Cells
Grid 1	80
Grid 2	120
Grid 3	270
Grid 4	612
Grid 5	1020
Grid 6	1530

Table 3.1: Convergence tests for radial grid

of 7770, but it can be noticed from figure 3.8 that it is important to reach a compromise between computational cost and error done. Simulations with a number of cells greater than 1000 are surely more precise, but the numerical simulation are quite expensive.
The consideration made with pressure distribution are valid also for temperature, the central part of the channel remain hotter and the shock is well described around the 1000 cells, see figure 3.9.

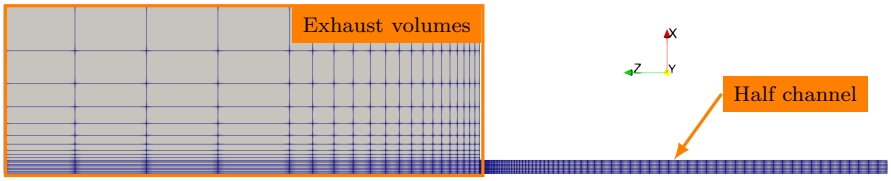

Figure 3.5: Mesh description

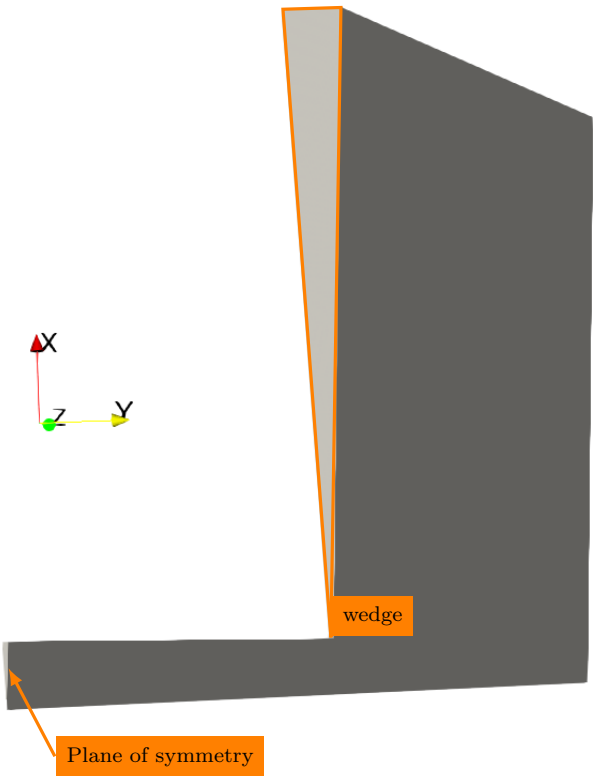

Figure 3.6: Axi-symmetric mesh, wedge patch

Figure 3.7: Mesh used for the radial convergence

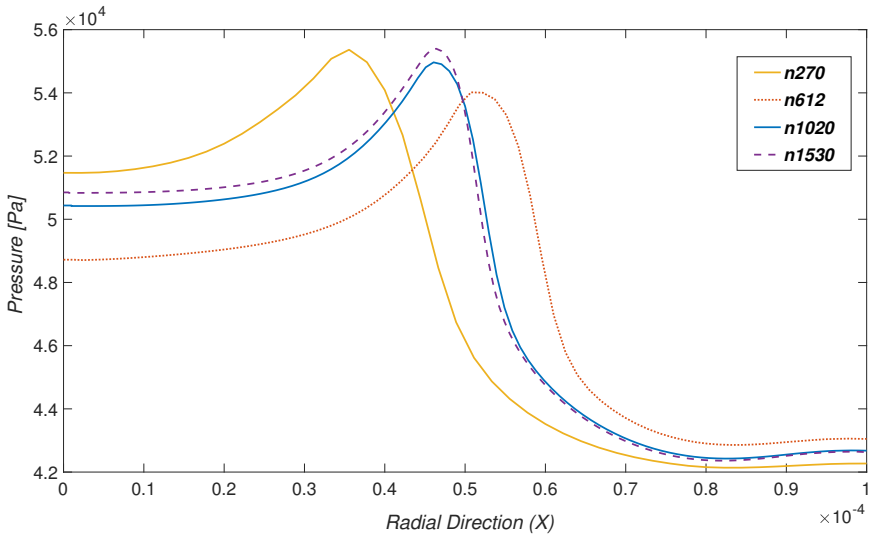

Figure 3.8: Pressure along radial direction at $t = 10^{-6}s$

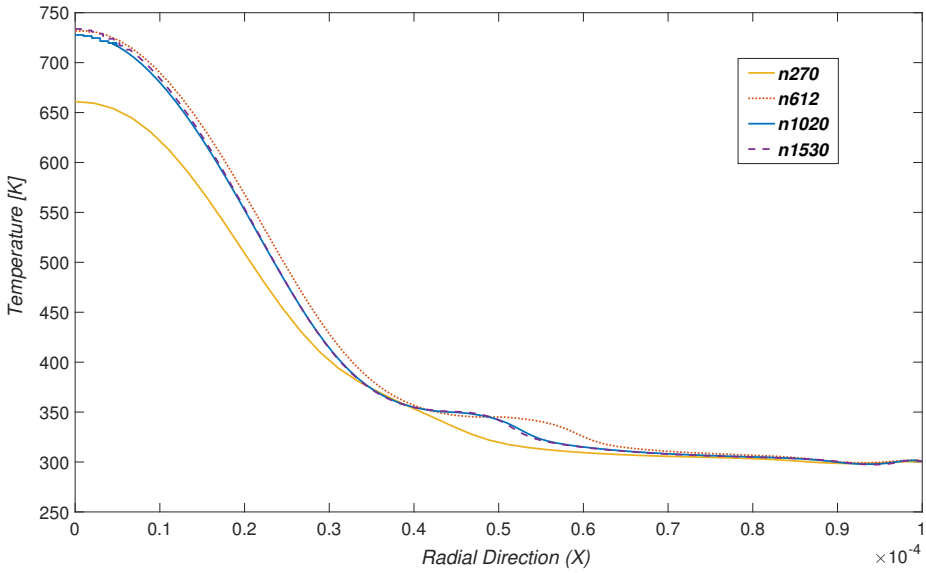

Figure 3.9: Temperature along radial direction at $t = 10^{-6}s$

3.3.2 Axial grid convergence

In axial direction things are different and particular attention should be payed to the outlets zone, it is crucial to capture strong gradients in terms of Mach number, pressure and temperature; the original mesh with the low-pressure chamber is now adopted. A smart choice could be a simple grading in the z-direction, with a coarse mesh in the middle of the channel and a dense one near the outlets (3.10)

```
simpleGrading
          ( 1  1
 (
 (50 50 20)
 (50 50 0.05)
 )
       )
```

This notation for simpleGrading states that in z-direction the mesh must be split in two parts, one with cells expansion rateo of 20 and the other one with 0.05, in figure 3.11 this parameter is explained.

In axial grid convergence three mesh were studied, results of second run are identical to third one, as it was said in section 3.3.1 when two run are

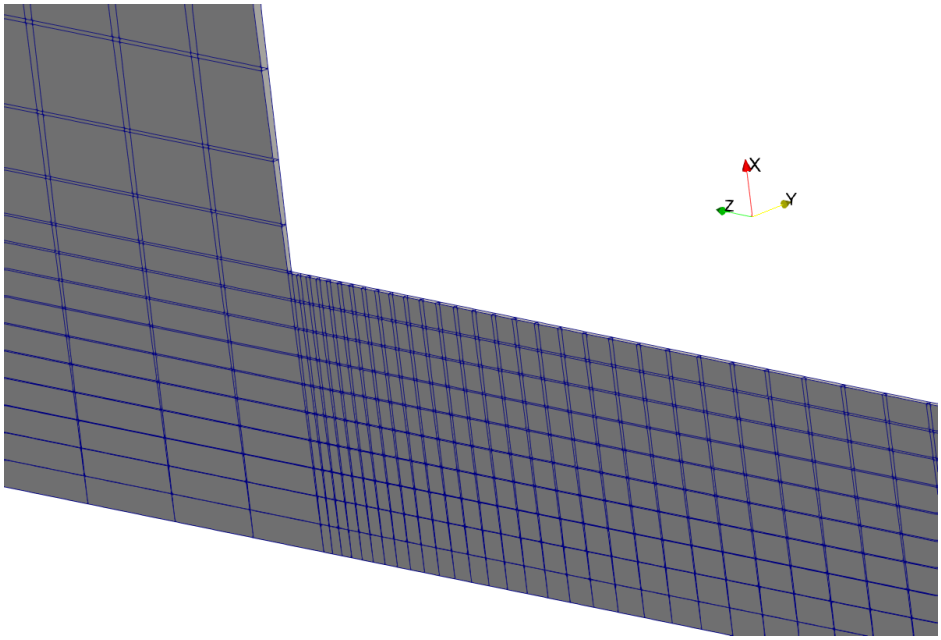

Figure 3.10: Mesh refinement near the outlets zone

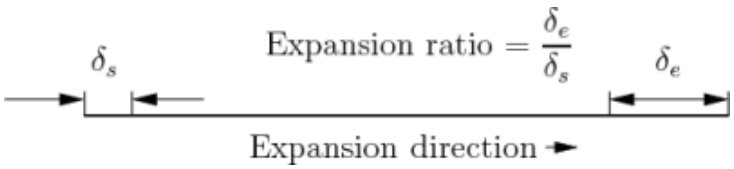

Figure 3.11: Mesh grading along a block edge

quite similar the grid chose is the more coarse, a progressive refinement is needed in axial direction while radial is kept with 10 cells, the number of cells in the simulation is pointed out in the following table:

Simulation	n Cells	Channel		Chamber	
		Radial	Axial	Radial	Axial
Grid 1	700	10	30	20	20
Grid 2	900	”	50	”	”
Grid 3	1150	”	75	”	”
Grid 4	1400	”	100	”	”

Table 3.2: Mesh characteristics for different simulations

Characteristic time in axial and in radial direction are deeply different, if the goal is to describe radial shock waves it is important to keep radial

refinement as it was studied, on the contrary, if the goal is to study the emptying channel is desirable to keep axial refinement and leave radial mesh quite coarse in order to obtain a good compromise between refinement and computational cost.

The analysis performed can drive the choice of the mesh towards two direction:

- If the main goal is to study fast phenomena like radial shock wave it is important to have at least 1000 cells with particular refinement in radial direction to fully capture shock path.
- On the contrary, if the main goal is to study slow phenomena like channel emptying the mesh needs to have at least 1150 with the radial direction left rather coarse.

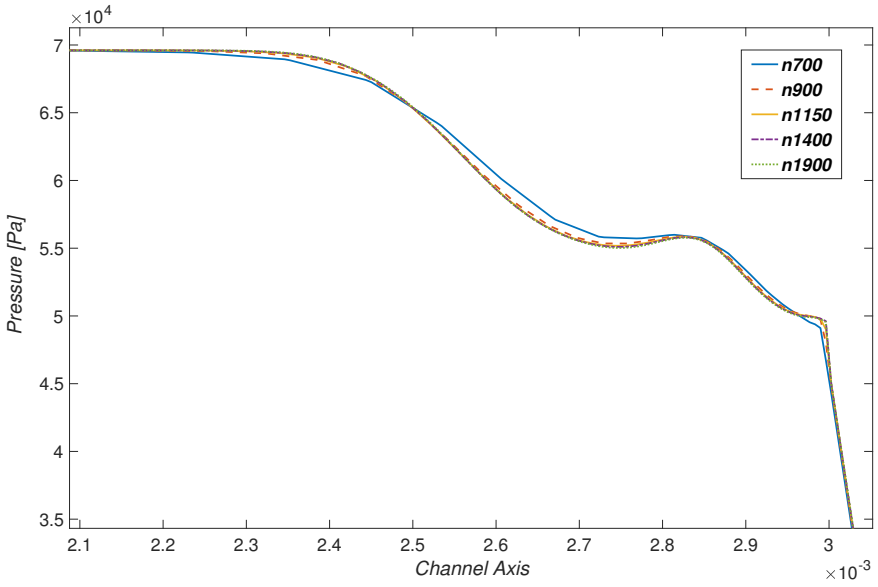

(a) *Pressure*

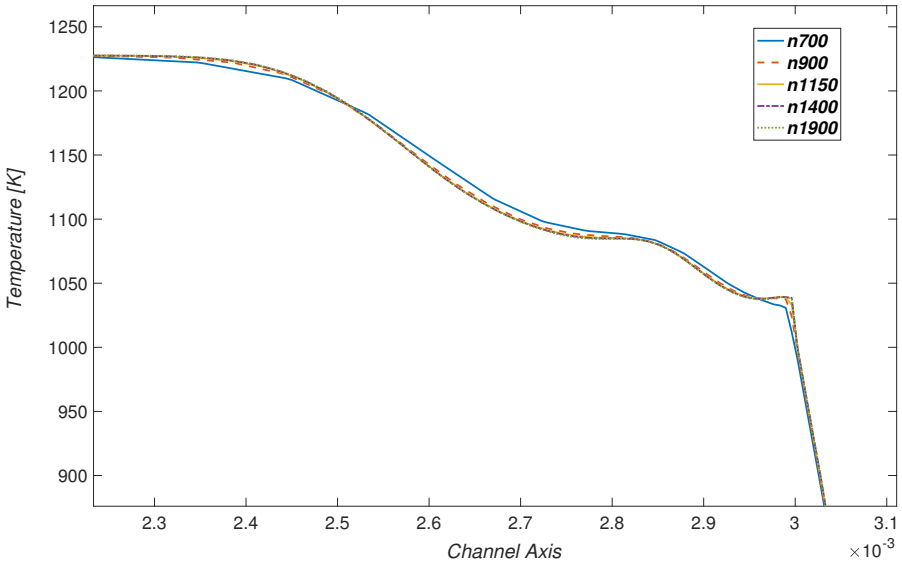

(b) *Temperature*

Figure 3.12: Pressure and temperature results from axial convergence

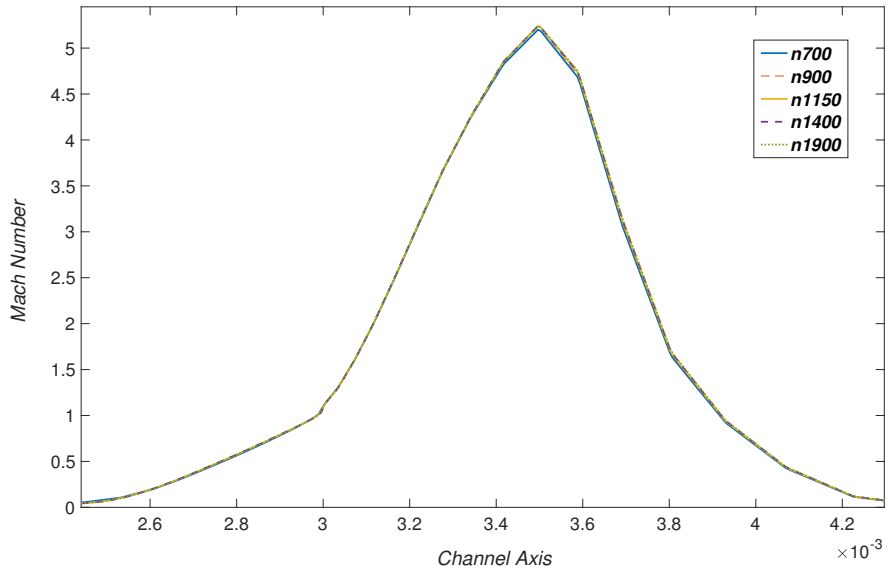

(a) *Mach*

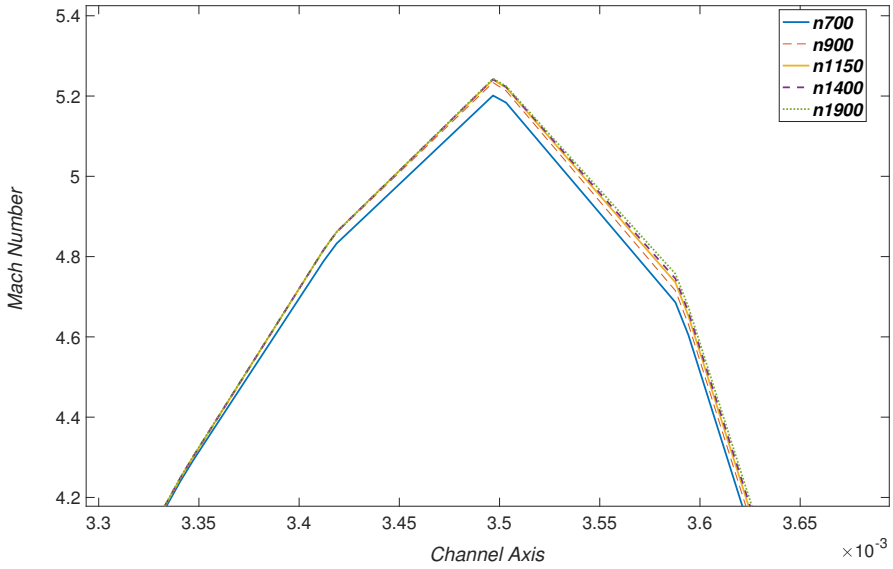

(b) *Mach zoom*

Figure 3.13: Mach number results from axial convergence

Chapter 4

Cases

4.1 Temperature set

One of the first question arising in radial grid convergence calculations is *how the cylindrical shock waves depends from initial temperature jump.* The aim of this section is to fully describe phenomena that occurs in radial direction. For this reason the adopted mesh is the one that comes from section 3.3.1, so very coarse in axial direction but extremely dense in radial direction.

Multiple simulations, thanks to utility `setFields`, are set with initial temperature that goes from $2000K$ to $18000K$, in the cylindrical portion of the heated gas and run till it is reached $1\mu s$.

Temperature $[K]$	Pressure $[Pa]$
2000	$2.77 \cdot 10^6$
4000	$5.54 \cdot 10^6$
6000	$8.31 \cdot 10^6$
8000	$1.10 \cdot 10^7$
10000	$1.38 \cdot 10^7$
12000	$1.66 \cdot 10^7$
14000	$1.94 \cdot 10^7$
16000	$2.21 \cdot 10^7$
18000	$2.49 \cdot 10^7$

Table 4.1: Initial condition in the cylindrical portion heated by laser

The main goal of these simulation is to see how radial shock waves drop with different initial temperature, for this reason all measurement are done in the middle of the channel along a line in the x-direction at $z = 0.03$ thanks to the utility `singleGraph`, it allows to write graph data for specified

fields along a line, specified by start and end points. The utility was set in order to catch 10000 points in x-direction in the middle of the channel including data for temperature, pressure and velocity field. Here is reported the configuration text file for this utility:

```
start   (0 0 0.003);
end     (0.0001 0 0.003);
fields  (T p U);

// Sampling and I/O settings
#includeEtc "caseDicts/postProcessing/graphs/sampleDict.cfg"

// Override settings here, e.g.
setFormat csv;

setConfig
{
    nPoints 10000;
}
```

The simulation set up can be summarized :

- Simulation run till 1e-6s saving results every 1e-8s
- Closed outlets and *slip* condition applied at new walls, the low pressure chamber is not present, it was seen emptying of channel is negligible at this time scale.
- Cylindrical portion of $r = 2.25 \cdot 10^{-5}$ heated by the laser, changing in T and P in setFieldsDict
- Temperature set increasing of 2000K
- Grid with 1020 cells, coarse in axial direction and dense in radial direction as shown in figure 4.2
- Total time of the simulation goes from 25 to 32 minutes

Figure 4.1 show the initial temperature profile for the T12000 simulation, as said before mesh in axial direction is quite coarse and a fixed value condition ($300K$) at the wall is applied, it possible to see that a temperature gradient arise. However measurement are taken away from this temperature gradient.

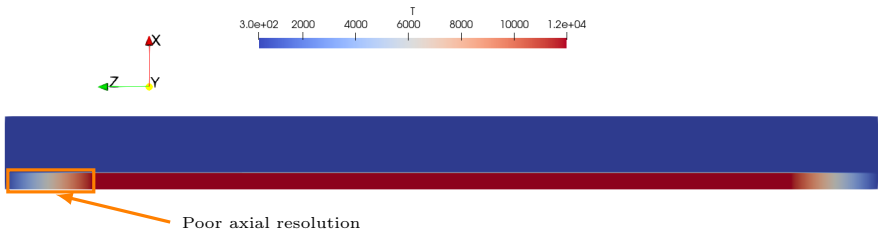

Figure 4.1: Temperature initial profile for simulation T12000

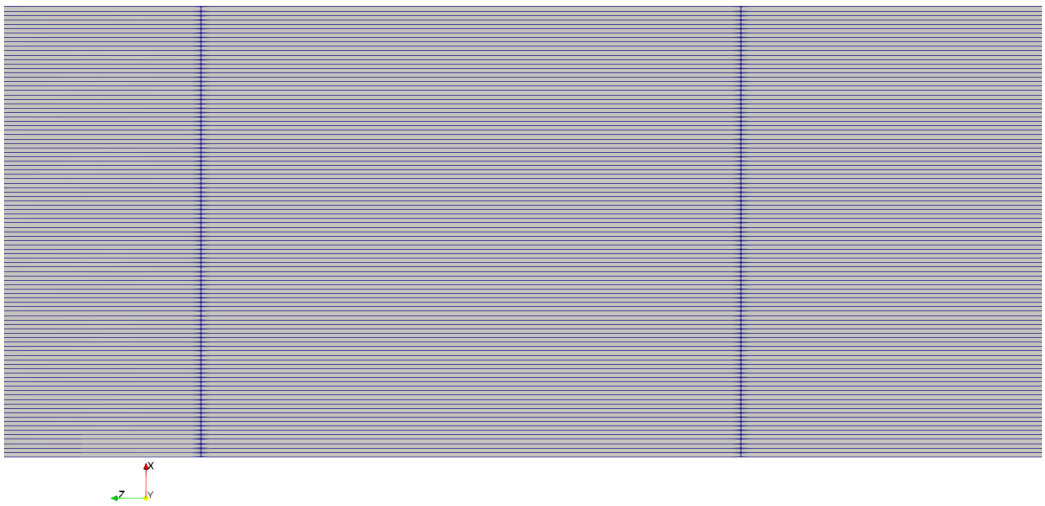

Figure 4.2: Mesh used for the simulation

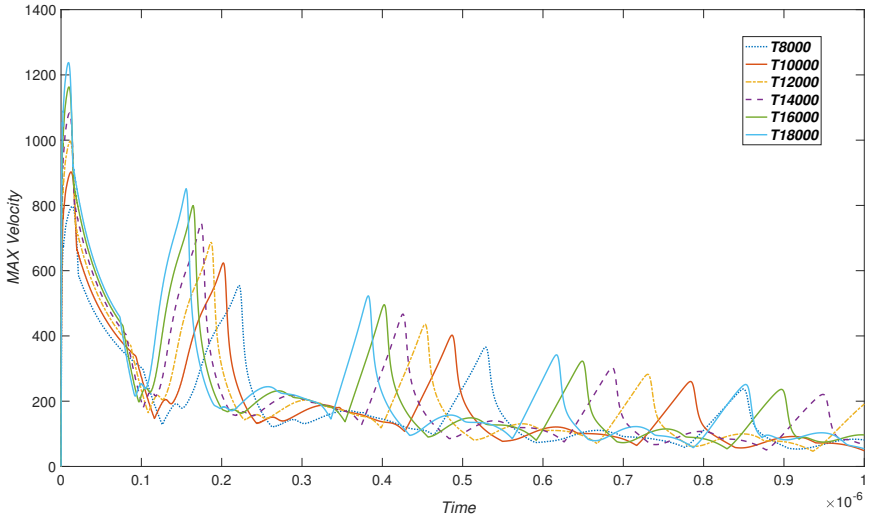

Figure 4.3: Maximum velocity in radial direction at different Temperature

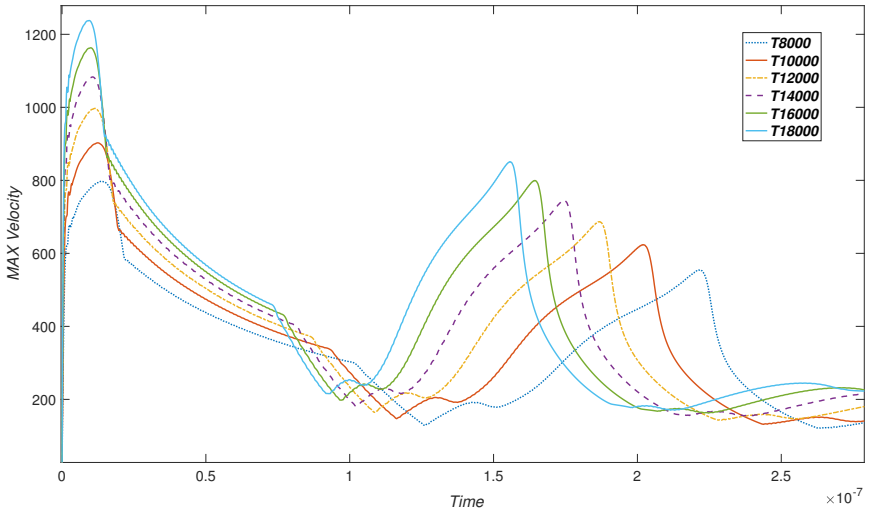

Figure 4.4: Focus on the first two bounces

For the sake of clarity only $T > 8000K$ are reported, for lower T the maximum velocity behaviour is not that interesting. As it can be seen from figure 4.3 and 4.4, peaks of maximum velocity seem to drop with an exponential decay whose time constant can be deduced by the curve fitting tool in Matlab; the idea is to find a correlation between temperature and oscillation drop. Results of figure 4.4 are reported in table 4.2.

Simulation		$\max V[m/s]$	Time $[s]$
T18000	1°	1238	9.4×10^{-9}
	2°	850.7	1.56×10^{-7}
T16000	1°	1163	1.02×10^{-8}
	2°	799.4	1.64×10^{-7}
T14000	1°	1083	1.07×10^{-8}
	2°	744.9	1.74×10^{-7}
T12000	1°	996	1.17×10^{-8}
	2°	685.5	1.86×10^{-7}
T10000	1°	902	1.24×10^{-8}
	2°	623	2.02×10^{-7}
T8000	1°	797	1.38×10^{-8}
	2°	554.6	2.22×10^{-7}

Table 4.2: Results of figure 4.4

From τ can be calculated the *half-life* $t_{1/2}$, it states the time required for a quantity, here maximum velocity, to reduce to half of its initial value:

$$t_{1/2} = \tau \, ln2 \tag{4.1}$$

The fitting curve is

$$V_{max}(\, T\,) = A_0 \, e^{-\lambda \, T} \tag{4.2}$$

In table 4.3 the values for λ are used to find $\tau = 1/\lambda$

Once found $t_{1/2}$, it is convenient to plot this quantity as function of temperature, again it is required the curve fitting tool in Matlab. The functional relationship between the half-life and temperature is a power law:

$$t_{1/2}(\, T\,) = a \cdot T^b \tag{4.3}$$

$$b = -0.406 \tag{4.4}$$

Temperature $[K]$	λ
2000	8.526×10^5
4000	1.077×10^6
6000	1.286×10^6
8000	1.495×10^6
10000	1.675×10^6
12000	1.832×10^6
14000	1.979×10^6
16000	2.112×10^6
18000	2.122×10^6

Table 4.3: Time constant value for different temperature

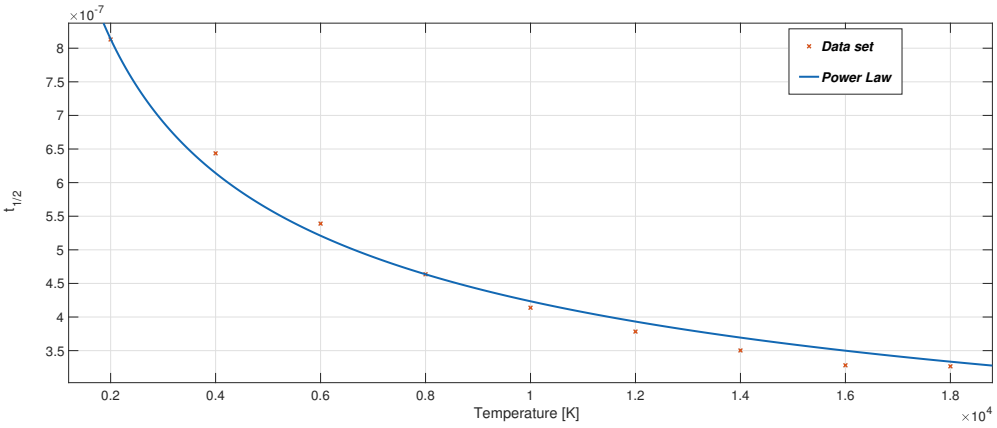

Figure 4.5: Power law for half-life at different temperature

This result can be explained looking at cylindrical shock behavior. Obviously higher the jump in pressure and temperature is, higher the velocity peak in the initial moments will be, leading to a faster damp in maximum velocity peak. The energy change in radial direction is due to cylindrical shock waves till $1\mu s$, later on is due to convection, this information states the simulation can be divided in two parts:

- Before $1\mu s$ when only radial phenomena are important and channel emptying is negligible.

- After $1\mu s$ when channel emptying is the leader player and radial shock wave are damped.

4.2 Channel Emptying

The main goal of this work is to understand if the set up of the experiment needs to be modified in order to obtain a coherent source of XUV for a consistent time. After the first emission argon leaves the channel and fresh new gas is introduced to begin a new cycle, the problem is that laser emission frequency is fixed $f = 100kHz$ and exist the possibility that the second cycle of gas introduction encounter gas still in expansion modifying the desired density profile. This problem is crucial since it can ruin the experiment, a careful evaluation of the emptying time is needed considering different initial temperature and channel diameter, paying particular attention to the flow rate that can give interesting information about the flow regime.

The simulation are run with the following set up:

- The mesh selected is the one that comes from axial grid convergence simulations discussed in section 3.3.2, the radial direction is left quite coarse, capture the shock waves is not of our concern at this point. So the mesh is made of 1150 cells, most of them are in the channel, some grading is necessary to grasp the flow features near the outlet.
- Duration of the simulation is crucial, there is no need to reach large time so an end time of $10^{-4}s$ is sufficient to predict the flow behaviour, results are saved every $10^{-5}s$
- Different initial temperature to simulate the laser beam heating the gas, from $6000K$ to $18000K$ listed in table 4.4. Starting from the chosen temperature the equation of state is used to calculate pressure of heated gas, density does not change during this process.
- Low pressure chamber always at $P = 100Pa$

OpenFOAM through the function `volFieldValue` provides options to manipulate volume field data into derived forms, for example to report summations, averages and volume integral. The operation performed is exactly `volIntegrate` in a specified region called channel defined previously, the volume integral of ρ inside the micro channel is performed every time step and saved in a specific postProcessing folder.
Another interesting parameter is the *mass flow rate* ϕ that can be calculated through the function `surfaceFieldValue` integrated in OpenFOAM, it provides options to manipulate surface field data into derived forms, in this work it is implemented to calculate the flow rate across a patch. The

Simulation	Gas		Laser-Gas	
	Temperature $[K]$	Pressure $[Pa]$	Temperature $[K]$	Pressure $[Pa]$
T18000	300	4.16×10^4	18000	2.49×10^6
T16000			16000	2.21×10^6
T14000			14000	1.94×10^6
T12000			12000	1.66×10^6
T10000			10000	1.38×10^6
T8000			8000	1.10×10^6
T6000			6000	8.31×10^5

Table 4.4: Initial setup of the simulations for channel emptying

patch is defined in the `topoSetDict` located in the system folder, thanks to this dictionary it is possible to define different zones, in this case is defined a faceSet that includes the cell faces adjacent to the low pressure chamber, so the outlet of the micro channel (figure 4.6). The function surfaceFieldValue perform a summation through the cell faces to obtain the global flow rate of the patches.

$$\phi_{tot} = 2\sum_{i=1}^{10} \phi_i = 2\sum_{i=1}^{10} \rho_i (U_z)_i A_i \tag{4.5}$$

This two functions are defined in a section of the controlDict, after the main parameter the `functions` are defined and performed every time step.

It is interesting giving a qualitative look at emptying process, after 1e-5 s part of the gas has already left the channel giving rise to a strong barrel shock in the low pressure chamber preceded by a rarefaction fan just after the outlets (figure 4.7); the intensity of the barrel shock progressively decrease till the end time of 1e-4 s when the channel is almost empty. Important fact is that the flow is always sonic at the outlet, this phenomena is called *sonic throat*, in other words gas cannot go over $Ma > 1$ because of the geometry of the channel: to further accelerate the flow a divergent cylinder is needed. So the flow is considered chocked and this is a big limitation for the channel emptying characteristics.

To compare results from the simulation it was used an emptying parameter $\frac{m}{m_0}$ where $m_0 = 1.74 \times 10^{-13} kg$ indicates the initial mass of gas in the channel and it is the same in every simulations. In plot 4.9 it is shown how the parameter $\frac{m}{m_0}$ change with time, we observe two important aspects:

- Gas with higher initial temperature leaves the channel faster than a gas with lower temperature, this because the pressure jump is higher

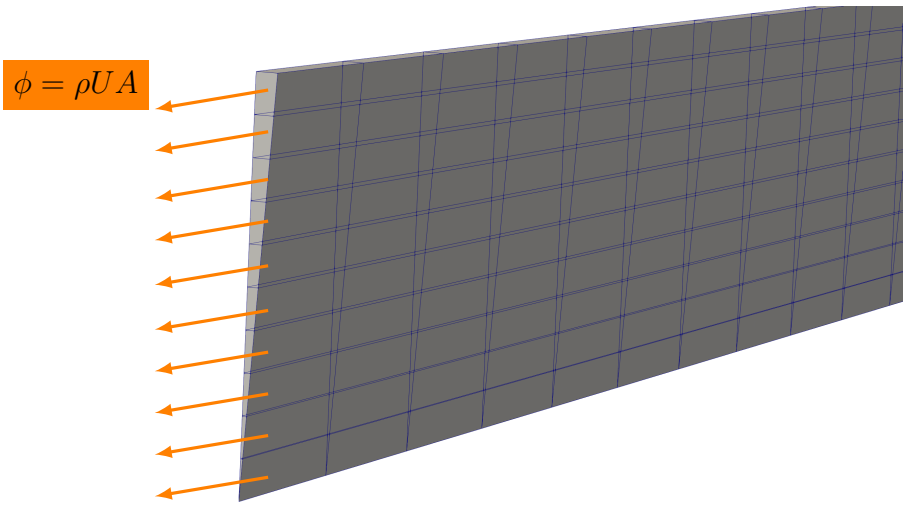

Figure 4.6: FlowRate

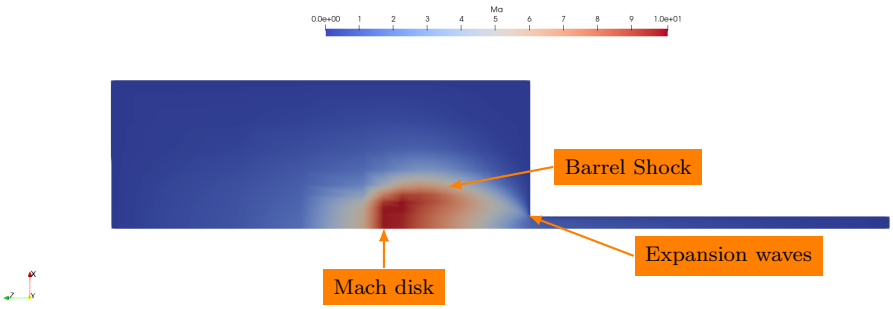

Figure 4.7: Emptying channel for T12000 after 1e-5 s

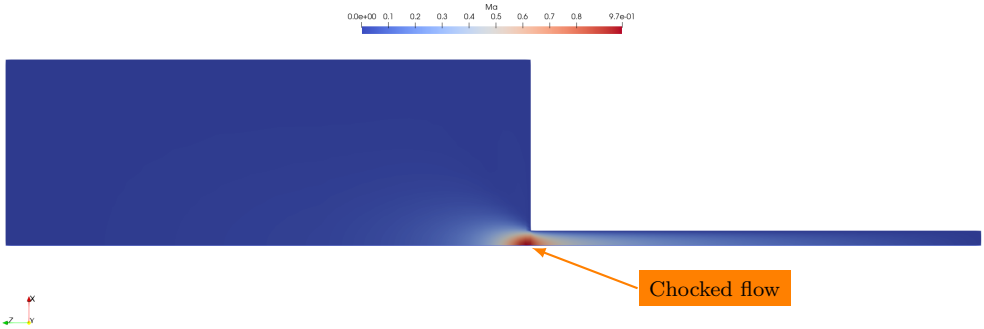

Figure 4.8: Emptying channel for T12000 at the end time of 1e-4 s

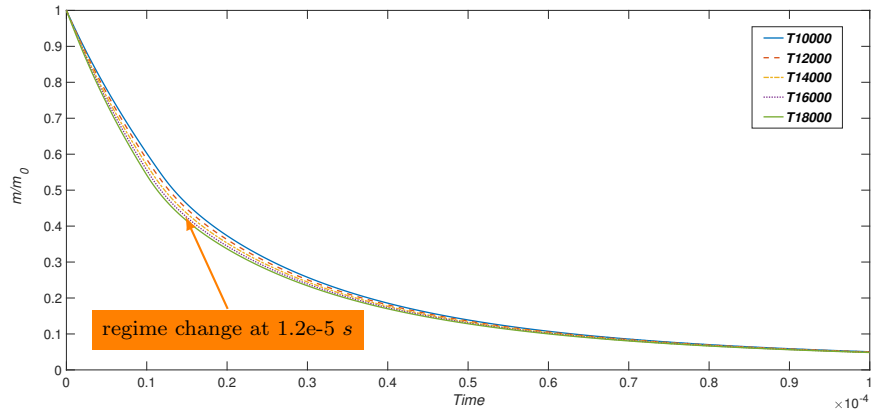

Figure 4.9: Emptying of micro channel

at the beginning of the simulation.

- At $t = 1.2 \times 10^{-13}$ the regime is changing, this is clear looking at the change of slope, but it would be clearer looking at the flow rate.

It is clear from figure 4.9 that there is not a substantial improvement increasing gas temperature, the channel will empty faster but not enough to justify a change in the set up, this could be demonstrate plotting the time constant τ as function of temperature. For this purpose it is used the curve fitting tool in MatLab to build the exponential fit, in this case it is a fit with two exponential to better capture the curve behaviour.

$$\frac{m(t)}{m_0} = M(t) = Ae^{Bt} + Ce^{Dt} \tag{4.6}$$

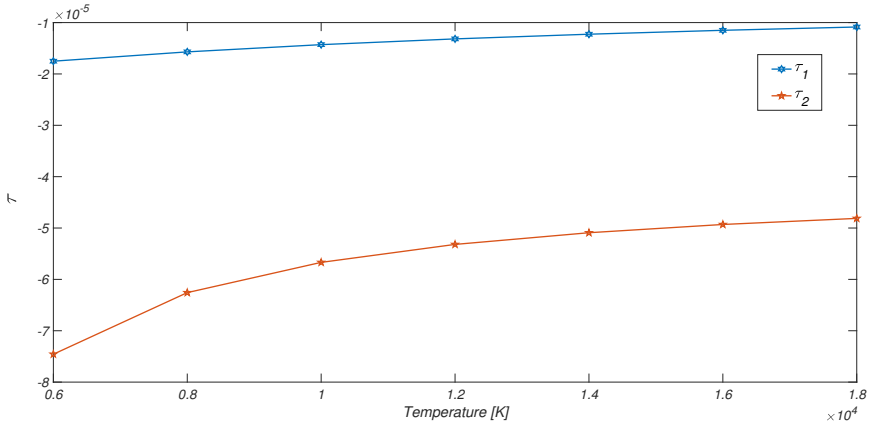

Figure 4.10: τ as function of temperature

The time constant τ is defined as

$$\tau_1 = \frac{1}{B} \qquad \tau_2 = \frac{1}{D} \tag{4.7}$$

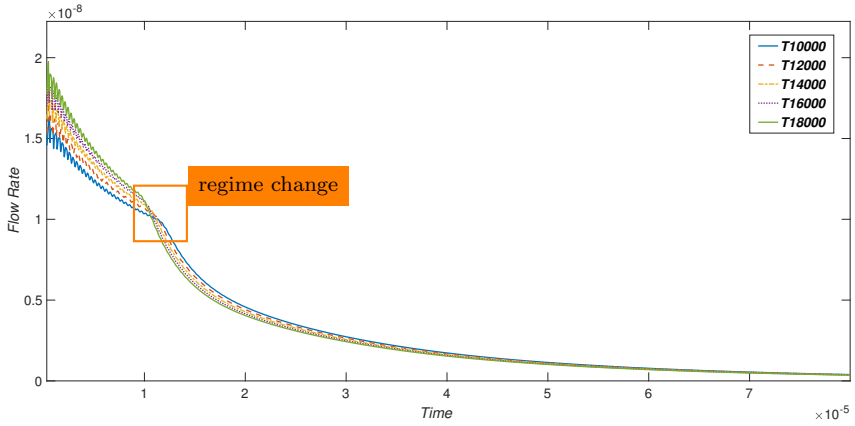

Figure 4.11: Flow rate for different simulations

As we can see in figure 4.10 the time constants don't change too much if the temperature increases, this means the process of emptying the channel is not strongly influenced by laser temperature. Figure 4.12 shows that temperature along channel axis change slightly from the first to the last simulation (at the end of the channel). Of course a major difference is noticed after $10^{-5}s$ because the center of the channel is the hottest part because heated

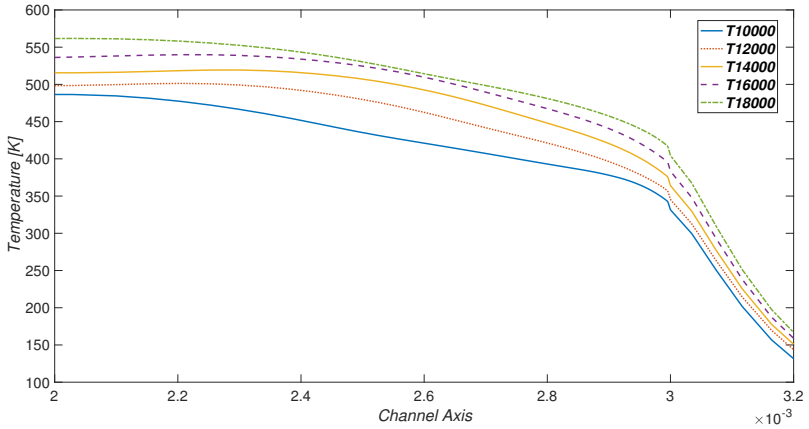

(a) $t = 10^{-5}s$

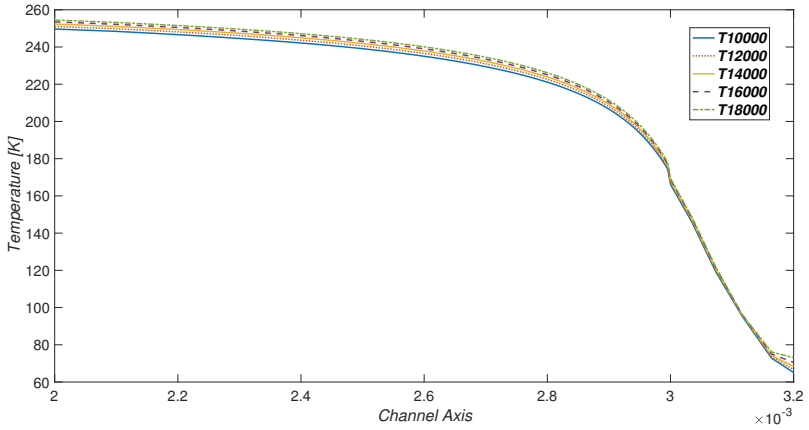

(b) $t = 5 \times 10^{-5}s$

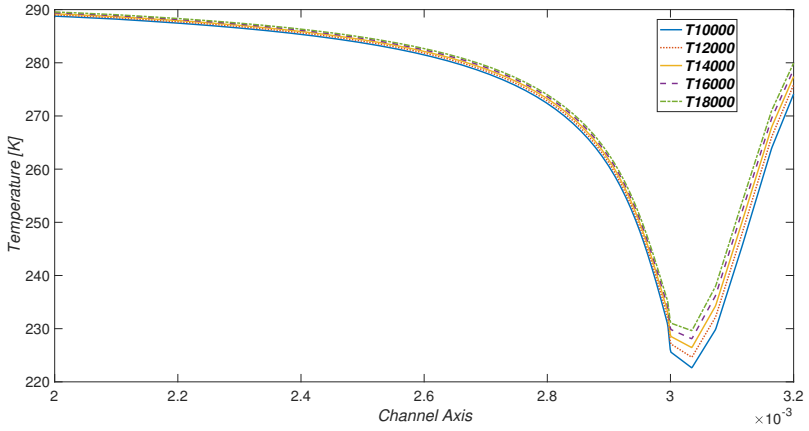

(c) $t = 10^{-4}s$

Figure 4.12: Temperature profile near the outlet at different time

up by the laser. After $10^{-4}s$ the differences are flatten, a positive feedback is given by figure 4.9 where it can be seen that after $5 \times 10^{-5}s$ the emptying of the channel does not depend on the initial temperature, but remains the same for all simulations.
Another interesting parameter is the flow rate, figure 4.11 show that in the first part of the simulation the flow rate present an oscillatory behaviour due to the radial cylindrical shock waves that propagates inside the channel, it was analysed in section 4.1 that radial phenomena are fast compared to the emptying channel and drop after $10^{-6}s$, this is correct but only partially: in *complete* simulation it is evident that radial shock waves are progressively weaker and weaker after this time, but they can be considered extinguished after $1.2 \times 10^{-5}s$ where it can be seen the regime changing. Clearly this behaviour is best explained by figure 4.11 where the oscillatory behaviour is captured, instead figure 4.9 represent an integral quantity and oscillation are averaged and "flatten" by the integral operator.

4.3 Effects of channel diameter

Changing the initial laser temperature did not produced the expected results, however it is possible to reduce the emptying time following a different path. Increasing the diameter will decrease impedance of the channel allowing a faster emptying process; it is important to underline that this path cannot be traversed since the chip dimensions are fixed, but it is analysed for information purposes. Four different configuration are analysed without modifying the mesh refinement.
The simulation set up is the following:

- The mesh selected is the one obtained in the axial convergence analysis, already used in the previous chapter, made of 1150 cells with grading near the outlet.

- Time control is kept unaltered from channel emptying simulations, so results are saved every $10^{-5}s$ and simulations end at $10^{-4}s$.

- Radius of the channel is changed during different simulations, the reference value is $100\mu m$ and a lower value of $75\mu m$ is tested along with higher value of $150\mu m$ and $200\mu m$.

- low pressure chamber is present with $P = 100Pa$

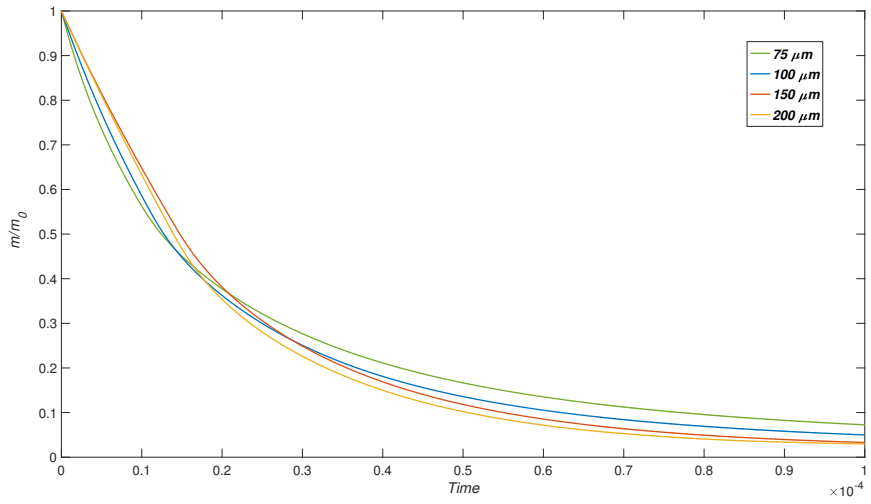

Figure 4.13: Mass fraction in the channel

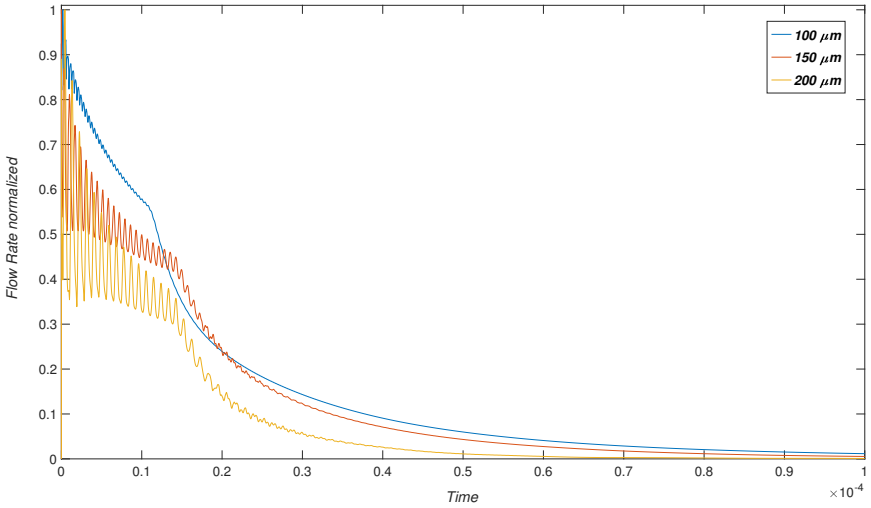

Figure 4.14: Flow rate with different diameter

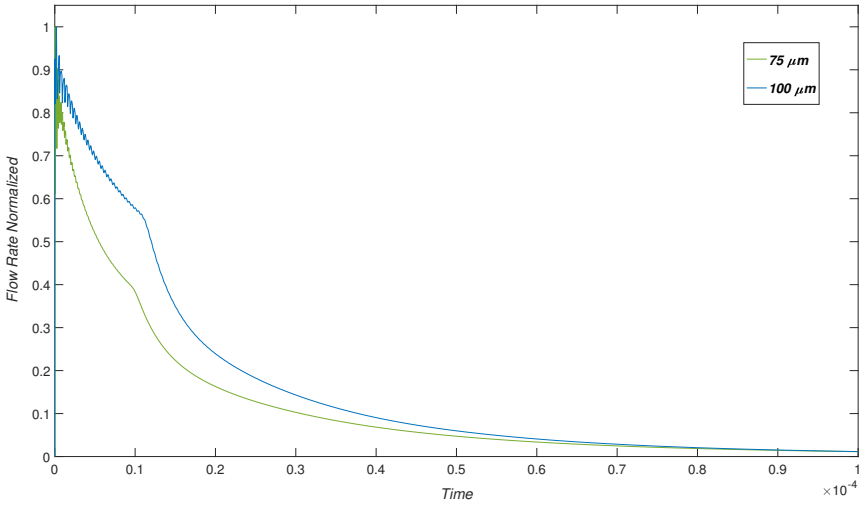

Figure 4.15: Flow rate reducing the diameter

Simulations confirm the hypothesis made in first instance, channel impedance is inversely proportional to the channel diameter. In figure 4.13 this behaviour is represented, as in section 4.2 the parameter considered is $\frac{m}{m_0}$ as function of time. It is clear that channel emptying for the $200\mu m$ test is the fastest, it should be noticed that, the more the diameter increase, the steeper is the slope in proximity of the changing regime . Initially the fastest channel are the smaller one, but when the regime changes (see section 4.2) at $10^{-5}s$ behaviour is inverted.
Special mention should be made for the flow rate

$$\phi = \iint_A \rho \mathbf{U} \; d\mathbf{A} \tag{4.8}$$

The analysis on this quantity start saying that the plotted quantity is the ratio between the flow rate and the maximum value reached, in fact the flow rate should be normalized in order to be compared.

$$\phi_{norm} = \frac{\phi}{\phi_{max}} \tag{4.9}$$

In figure 4.14 it can be seen that bigger radius consists in higher flow rate oscillation and a delay in the changing regime, this is probably due to the late drop in radial shock waves. On the contrary the steepness of the curve is smaller meaning a quicker emptying process. Observing figure 4.15 it is evident a smaller channel has the quality of reducing oscillatory phenomena

that worsen the emptying process, but the best performance concerning flow rate is obtained with the reference value of $r = 100\mu m$. In conclusion it is important to underline that the flow rate is not the main parameter to select the more appropriate configuration, it is more important the ratio between mass in the channel and initial mass.

4.4 Mechanical loads on channel wall

From an engineering point of view it should be interesting analyse the pressure on the chip, gas pressure and density are quite low at the beginning of the test, when argon is hit by laser impulse it immediately increases its temperature and pressure, for this reason it is studied the pressure and forces acting on the glass chip that would drive the HHG. Here is reported the set up of this simulation:

- The only temperature tried is an intermediate $T = 12000K$ for the laser hit section, pressure in this region reach $P = 1.66 \times 10^6 Pa$ while in the rest of the channel $T = 300K$ and $P = 4.16 \times 10^4 Pa$.
- Mesh is the one used for channel emptying analysis with a diameter of $100\mu m$ and no more meshes are tested for this simulation. Number of cells are 1150 with gradient near the outlet.
- Duration of the simulation is set for $10^{-4}s$ and every time step of $10^{-10}s$ a result of forces and momentum on the top wall of the channel is saved.

The function adopted is the one called `forces` that allow to calculate forces and momentum on a specified patch or region, in this case the chosen patch is the top wall of the channel.

```
forces1
  {
   type            forces;
   libs            ("libforces.so");
   log     true;
   patches         (WallChannel);
   CofR     (0 0 0);
   writeControl    writeTime;
  }
```

Saving the results every time step generates a huge file, but it helps observing the oscillatory behaviour of pressure inside the channel due to radial

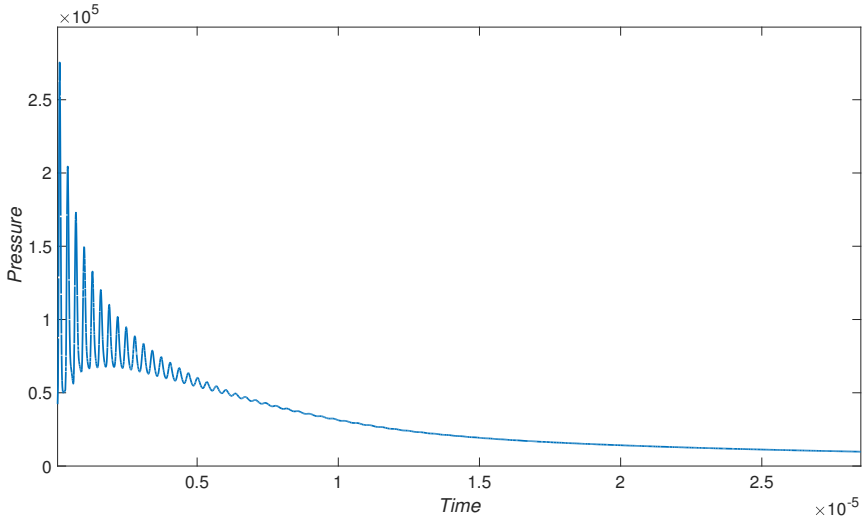

Figure 4.16: Pressure over time on the chip for $T = 12000K$

cylindrical shock waves. In the .dat file saved in the postProcessing folder it can be found sum of forces in direction x, y and z, viscous forces (negligible in this problem) and sum of moments that are not of particular interest. The attention is focused on force in x direction, so normal to the wall. To retrive pressure it is necessary the patch area $A = 5.23 \times 10^{-9} m^2$ and the performed operation is $P = \dfrac{F_x}{A}$

Figure 4.16 shows results of simulation T12000 where the laser heats the gas till $12000K$. Maximum pressure on the wall arise in the first instant of the simulation, it reaches 2.7 bar almost six and a half time the initial pressure inside the channel, pressure on the chip quickly drop and stabilise around 0.2 bar after $1.2 \times 10^{-5} s$ when the radial shock waves drop. This results can be a starting point for future analysis on chip manufacturing and shape configuration, of course model should be improved but this result give a clue on the intensity of the phenomena.
In figure 4.17 and 4.18 are shown respectively results from the lower ($8000K$) and higher ($18000K$) temperature set. It is clear that with an higher initial temperature, the maximum pressure on the chip will increase.

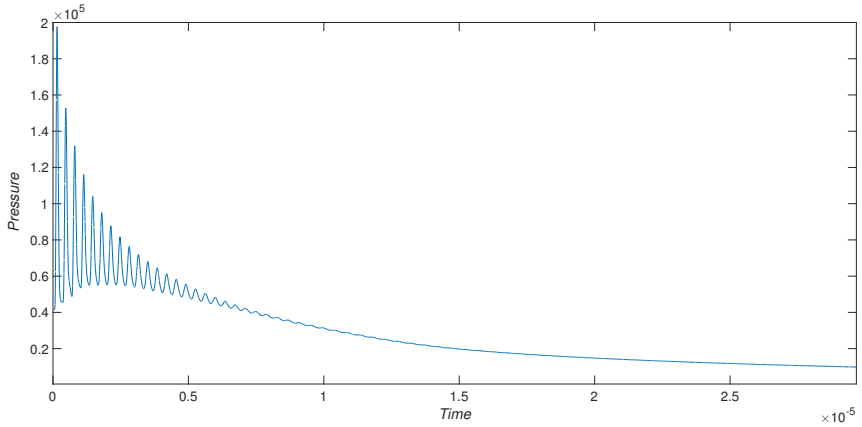

Figure 4.17: Pressure over time on the chip for $T = 8000K$

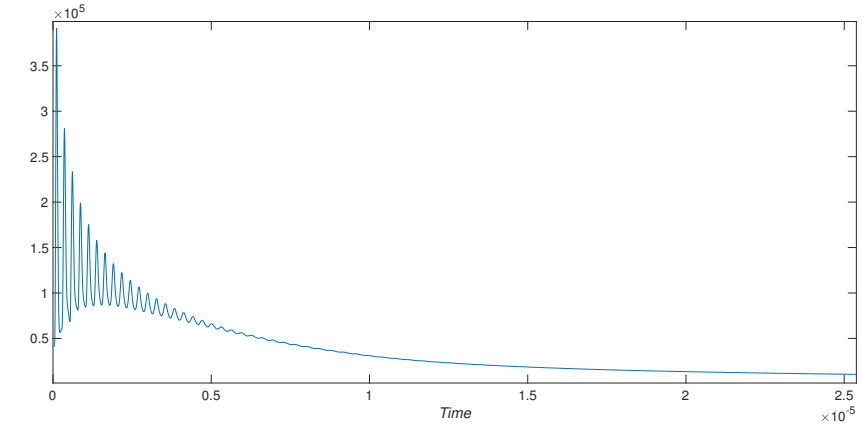

Figure 4.18: Pressure over time on the chip for $T = 18000K$

4.5 Thermal loads on channel wall

The heat flux or thermal flux is a flow of energy per unit area per unit of time. In SI its unit are Watts per square meter $\left(\frac{W}{m^2}\right)$. Heat is transported mainly by conduction and heat flux is described by Fourier's law:

$$\Phi_q = -k\nabla T \tag{4.10}$$

Figure 4.19 shows the power loss at the channel wall, the negative sign indicates that power flux goes outside the channel, a strong hypothesis is made: a fixed temperature value is put on the channel wall $(300K)$.

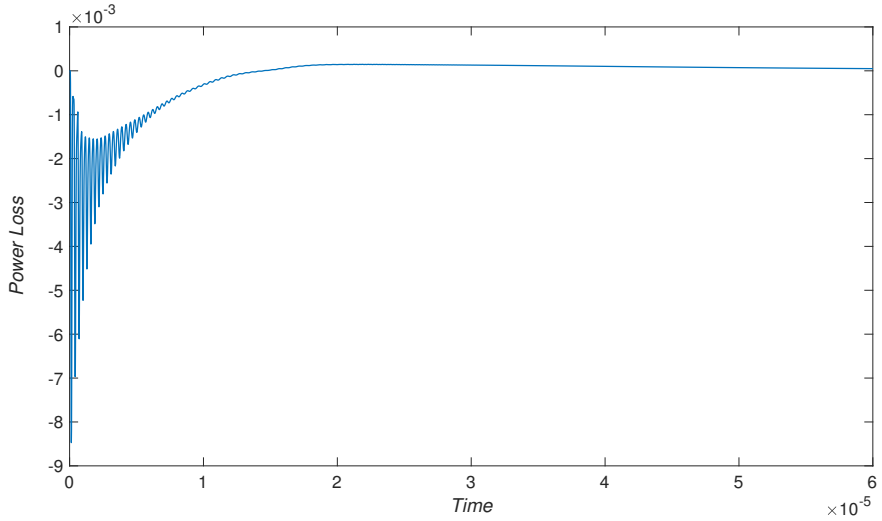

Figure 4.19: Power loss $[W]$ at wall channel for $T = 12000K$

These results, even if not relevant because of hypothesis adopted, can be a good starting point in analysing energy balance, we can forecast the time rate of change of energy in a physical system.
In figure 4.20 and 4.21 it is represented the power loss for an initial temperature of $8000K$ and $18000K$

Thermal flux at the wall is an interesting result and deserves a mention in this section. Figures 4.22, 4.23 and 4.24 show the maximum thermal flux at the channel wall, the oscillatory trend due to radial shock waves vanishes rapidly, in the order of $10^{-5}s$

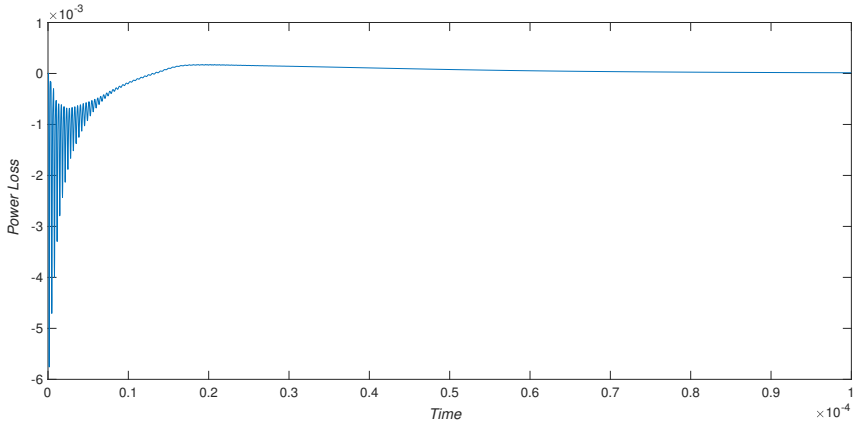

Figure 4.20: Power loss $[W]$ at wall channel for $T = 8000K$

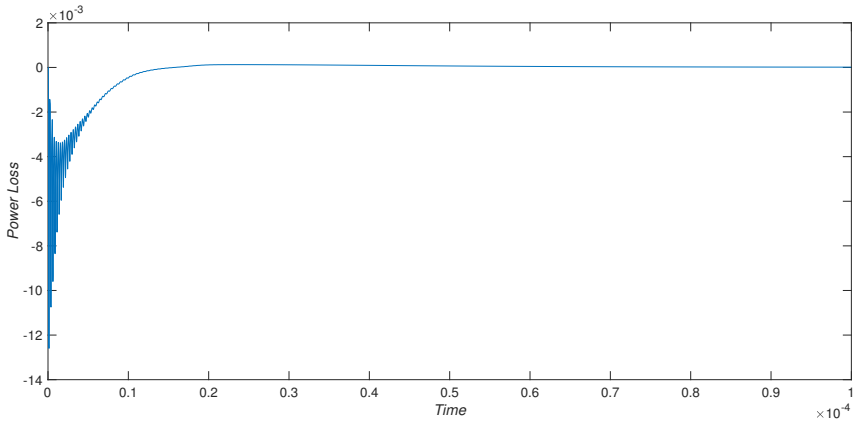

Figure 4.21: Power loss $[W]$ at wall channel for $T = 18000K$

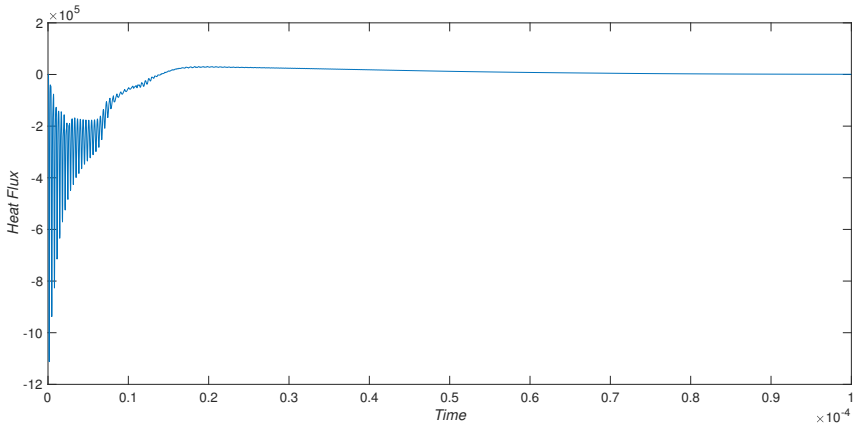

Figure 4.22: Heat flux $[W/m^2]$ at wall channel for $T = 8000K$

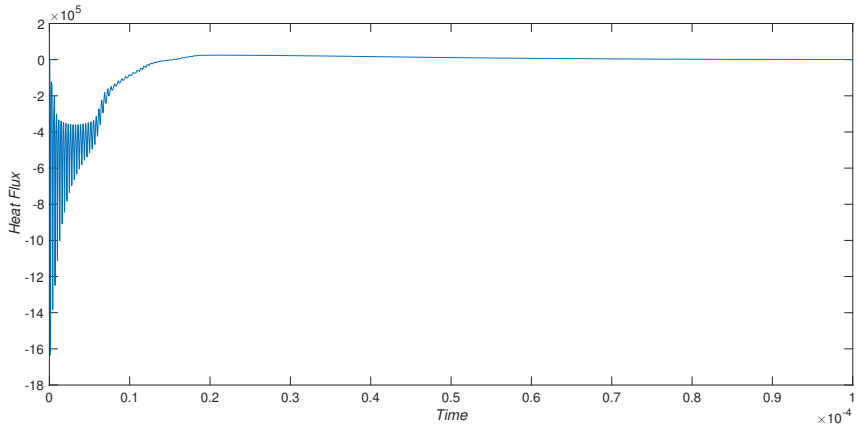

Figure 4.23: Heat flux $[W/m^2]$ at wall channel for $T = 12000K$

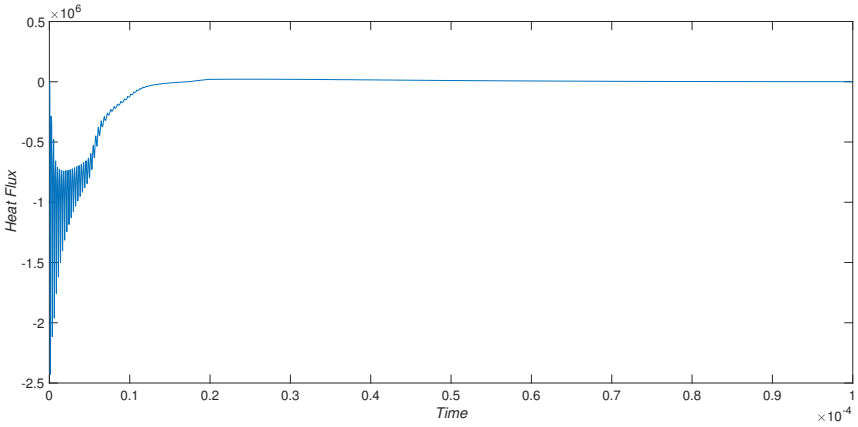

Figure 4.24: Heat flux $[W/m^2]$ at wall channel for $T = 18000K$

Chapter 5

Conclusions

The main goal of this work is to simulate Argon behaviour, after the interaction with an high energy laser impulse in a micro channel. Through the numerical analysis performed by OpenFOAM different situations are studied. Particular attention is given to the events happening in the first moments, so radial shock waves due to high pressure and temperature gradient. It is found that characteristic time of this phenomena is in the order of $1 - 12\,\mu s$ and their intensity is directly proportional to channel diameter.
The main focus of the study is to assess the channel emptying time because of laser impulse limitation: it can operate at the maximum frequency of $100kHz$ and the laboratory set up cannot be changed. It is found that the emptying time is too slow compared to laser maximum frequency and a different laser set up or chip geometry should be considered. Analysis on different laser temperature shows a little improvement, but it is not enough to empty the channel in less than $10\mu s$.
Further considerations are made on forces generated on the chip and on heat fluxes at the wall, it is found that pressure increase by 7 times compared to initial pressure in the channel, but drops quickly and after $1.5 \times 10^{-5}s$ returns to previous value and even lower. Heat fluxes at the wall is reported for completeness but it is not a significant data, it is clear that major power loss happen in the first instance when radial shock waves are present.
Future developments can focus on building a better model, the complete geometry with supersonic gas inlet should be studied in detail along with a better treatment of laser-gas interaction.

Bibliography

[1] M Chase. *NIST-JANAF Thermochemical Tables, 4th Edition*. American Institute of Physics, -1, 1998-08-01 1998.

[2] AG Ciriolo, R Martínez Vázquez, V Tosa, A Frezzotti, et al. High-order harmonic generation in a microfluidic glass device. *Journal of Physics: Photonics*, 2(2), 2020.

[3] A.G. Ciriolo, Rebeca Martínez Vázquez, Alice Roversi, Frezzotti Aldo, et al. Femtosecond laser-micromachining of glass micro-chip for high order harmonic generation in gases. *Micromachines*, 11(2):165, 2020.

[4] The OpenFOAM Foundation. Openfoam v8 user guide. `https://cfd.direct/openfoam/user-guide`.

[5] Ferenc Krausz and Misha Ivanov. Attosecond physics. *Reviews of modern physics*, 81(1):163–234, 2009.

[6] Alexander Kurganov, Sebastian Noelle, and Guergana Petrova. Semidiscrete central-upwind schemes for hyperbolic conservation laws and hamilton–jacobi equations. *SIAM Journal on Scientific Computing*, 23(3):707–740, 2001.

[7] Randall J. LeVeque. *Numerical methods for conservation laws (2. ed.)*. Lectures in mathematics. 1992.

[8] Muhammad Nurhuda, Akira Suda, Masatoshi Hatayama, Keigo Nagasaka, and Katsumi Midorikawa. Propagation dynamics of femtosecond laser pulses in argon. *Physical Review A*, 66(2):023811, 2002.

[9] Stephen B Pope. *Turbulent flows*. Cambridge Univ. Press, Cambridge, 2011.